THE PENNSYLVANIA STATE UNIVERSITY
SCHREYER HONORS COLLEGE

DEPARTMENT OF BIOENGINEERING

EXPERIMENTAL STUDIES OF THROMBUS FORMATION IN A BACKWARD FACING STEP

ANDREW T. CATHERINE
Spring 2011

A thesis
submitted in partial fulfillment
of the requirements
for a baccalaureate degree
in Bioengineering
with honors in Bioengineering

Reviewed and approved* by the following:

Keefe B. Manning
Associate Professor of Bioengineering
Thesis Supervisor

Peter J. Butler
Associate Professor of Bioengineering
Honors Adviser

Steven Deutsch
Senior Scientist Emeritus
Faculty Reader

* Signatures are on file in the Schreyer Honors College.

Abstract

Thrombus formation is a major consideration and concern in the design and use of implantable biomedical devices including cardiac assist devices and artificial heart valves. To better understand the conditions in which thrombi form and how fluid flows affect the geometry of resulting thrombosis, an *in vitro* backward facing step model and flow loop is used in combination with magnetic resonance imaging to obtain the geometry of formed thrombi. The simulations are performed with a pulsatile flow to simulate physiological conditions. The imaging is conducted after the flow loop has run for 15 minutes, 30 minutes, 45 minutes, and 60 minutes at a physiologically relevant flow rate to gain an appreciation for the transient development of the thrombus. Post-processing of the magnetic resonance imaging data is performed to create a mesh of the three-dimensional thrombus that will be used for computational fluid dynamic simulations. These studies showed that the thrombi begin to degrade almost immediately during MRI imaging in Phosphate Buffered Saline. The volume was calculated for a thrombus over a 195 minute period and clearly showed a decrease in size. Variations in blood flow time also produced a corresponding change in thrombi size where longer time periods produced larger thrombi.

Table of Contents

List of Figures

List of Table

Acknowledgments

First, I would like to thank Dr. Keefe Manning and Dr. Steven Deutsch for all of the guidance they has provided over the course of this research project. In addition, I would like to acknowledge George Long, Josh Taylor, and Andrew Higgins from the lab who have been instrumental in teaching and assisting me in my research.

Funding for this project was provided by a grant from the Grace Woodward Foundation and the Pennsylvania State University's Schreyer Honors College and College of Engineering.

I would like to thank Dr. Thomas Neuberger at the Huck Institutes Magnetic Resonance Center who worked with me for many hours during the project. His vast knowledge on MRI was a great resource.

Finally, I would like to thank Dr. Eric Patterson and Dr. Brent Craven from Penn State's ARL. Their background on CFD and meshing was extremely helpful in overcoming many of the obstacles encountered during this project.

Chapter 1

1.1 Introduction

Thrombus formation is a critical area of research in the design and use of implantable cardiac prosthetic devices. An important goal for improved designs is to understand the conditions under which thrombi are created and to predict the growth patterns and resulting size of such events.

1.2 Clinical Need

In the past 30 years, the number of patients suffering from heart failure and coronary artery disease has tripled [1]. Today there are over 5.8 million people in the United States with some form of heart failure [1-4]. Ventricular assist devices are one option for those waiting for a heart transplant or as a bridge to recovery device [1]. Over 500,000 new cases of heart failure are diagnosed annually in the United States, with 75 percent of those cases occurring in patients that do not meet the standards for a heart transplant [1]. Without a heart transplant or a ventricular assist device, less than 60% of patients survive more than 5 years [3].

To help fill this gap, ventricular assist devices are currently being used as the best treatment option for such patients [1, 5]. There is still a growing need to design better assist devices that extend the period of time a patient could survive while minimizing complications. A primary complication stems from the propensity for the current devices to cause thromboembolic events. In up to 25% of patients with left ventricular assist devices, thromboembolic events occur [6]. Even when patients are placed on anticoagulant medications, microembolic events still take place. Fortunately, the majority of patients with microemboli do not exhibit neurological symptoms, however,

these facts are evidence of the limitations anticoagulant therapies have with current cardiac assist device designs [6, 7]. Through better understanding of the fluid mechanics that create thrombi, the design of ventricular assist devices could be improved to reduce the incidence of thromboembolic events.

Cardiovascular device design could also benefit from a more complete understanding of thrombosis in prosthetic heart values, arterial stents, and arterial grafts. These devices suffer similar issues related to thrombosis as ventricular assist devices [8, 9]. The design of each type of device creates areas of stagnation and recirculation that increases a patient's risk of a thromboembolic event [10-12]. The risk associated with these cardiovascular implants could be reduced with an improved understanding of the associated fluid mechanics.

1.3 Previous Studies

Thrombosis is a natural defense mechanism that protects from blood loss [13, 14]. The mechanism of thrombosis is described by Virchow's triad which includes: blood constituency, material properties, and fluid mechanics [15, 16].

Blood constituency or the concentration of the individual components of blood impacts thrombus formation. For example, as a result of injury the coagulation cascade of factors and proteins promotes the polymerization of fibrinogen to fibrin and platelet aggregation to produce a thrombus [13]. This process varies among species and persons depending on their individual rheological profile [13, 17]. Among humans, variations in hematocrit and defects in the coagulation process as a result of different pathologies can increase the likelihood of a thromboembolic event [13]. Regulation and prevention of thrombus formation has been performed with some success by inhibiting factors in the coagulation cascade using medications [18].

The second component of Virchow's triad links thrombosis with the blood clotting surface [15]. In biomedical devices, obtaining biocompatibility is a highly important design consideration to minimize immune response, inflammation, and thrombosis [11, 19, 20]. The chemical properties and three-dimensional micro-structures of biomaterials are critical properties that must be examined to minimize adverse thrombotic events. By considering these biomaterial properties in the design of devices, the biological reaction to the artificial materials has been shown to be reduced [21, 22].

The third component of Virchow's triad accounts for the effects of fluid mechanics on thrombus formation. The bulk of this study examines how the fluid mechanics of blood flow impacts thrombus formation and development.

The analysis of blood flow is possible using the field of fluid mechanics. Fluid mechanics is described by a set of differential equations that account for the many different physical laws that govern fluid motion, such as the conservations of mass, energy, and momentum [23]. Conservation of mass leads to the development of the continuity equation for fluids as:

$$\frac{\partial \rho}{\partial t} + \vec{\nabla} \cdot \left(\rho \vec{V}\right) = 0 \quad \text{(Eqn 1)}$$

where ρ is the density of the fluid, t is time, ∇ is the gradient operator and, V is the velocity vector of the fluid.

Conservation of momentum across in an infinitesimal volume in the fluid domain is represented by Cauchy's Equation:

$$\frac{\partial}{\partial t}\left(\rho \vec{V}\right) + \vec{\nabla} \cdot \left(\rho \vec{V} \vec{V}\right) = \rho \vec{g} + \vec{\nabla} \cdot \sigma_{ij} \quad \text{(Eqn 2)}$$

where g is the gravity tensor and σ_{ij} is the nine component stress tensor describing stress exerted on the fluid.

Assuming that the fluid is Newtonian, incompressible and isothermal, its motion can then be described via the incompressible Navier-Stokes equation:

$$\rho\left(\frac{\partial\vec{v}}{\partial t}+\vec{v}\cdot\nabla\vec{\mathrm{v}}\right)=-\vec{\nabla}P+\mu\nabla^2\vec{v}\ \text{(Eqn 3)}$$

where P is the pressure and μ is the viscosity of the fluid.

To experimentally investigate thrombosis and fluid mechanics, a three-dimensional backward facing step was used. This design incorporates multiple recirculation zones, has been studied extensively, is relatively simple in geometry, and simulates flow patterns encountered in many cardiovascular devices [24-27]. Armaly et al. performed early studies on the backward facing step geometry, both experimentally and computationally, to determine the characteristics and areas of recirculation in the fluid flow [24]. There have been numerous papers since Armaly et al. examining the backward facing step at various Reynolds. Much of this advancement has been facilitated by computational fluid dynamic (CFD) modeling as is described in Section 1.5. The research to determine the size of the areas of recirculation and points of reattachment for various backward facing step expansions and Reynolds numbers conditions has previously been completed [28, 29]. This study will build upon this prior work to determine its affect on thrombus formation.

Figure 1-1 from Gresho et al. illustrates the streamlines of the flow downstream of a backward facing step [29]. There are two recirculation zones downstream of the step. The larger area of recirculation is on the bottom of the channel and the second smaller recirculation zone is located further downstream and at the top of the channel.

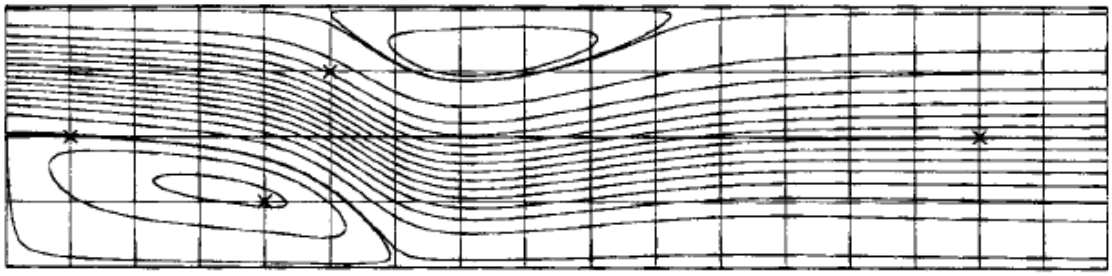

Figure 1-1: Streamlines of the fluid flow immediately downstream of a typical backward facing step (Reynolds Number =800) [29].

We seek to better understand the flow stresses that develop and cause thrombosis downstream of a backward facing step under physiologically relevant conditions.

Previous experiments have found that modeling thrombus formation with *in vitro* flow loop experiments is representative of the *in vivo* situation. In particular, early work done in 1958 by Chandler correlates thrombosis results from a simple *in vitro* model with *in vivo* results [30]. Later research has confirmed these results and built upon them to describe platelet activation in *in vitro* flow loops [31]. This study will use the previously described correlation between *in vitro* flow loops and *in vivo* flow conditions to represent the thrombosis process.

1.4 Thrombus Imaging

Magnetic resonance imaging (MRI) has been used as a non-invasive method of distinguishing atherosclerotic lesions and thrombi [32, 33]. This imaging technique is possible due to the difference in magnetic properties between blood and the surrounding tissue or model [32]. Johnstone *et al.* have used magnetic resonance imaging to image thrombosis in an *in vivo* rabbit model and found that the MRI images created an accurate representation of the thrombi [33]. Their study however had rather low contrast and image definition since thrombus formation in the rabbit model was not static [33]. The movement of the rabbit's blood during imaging and the slow change in the morphology

of the thrombi were the primary limitations of the Johnstone *et al.* study. Fayad *et al.* have also been able to achieve characterization via magnetic resonance imaging of atherosclerosis in the mouse model [32]. The *in vivo* model was a limiting factor in terms of spatial resolution for both studies. A reduction in resolution was caused by the external radio frequency coil having to encompass the entire animal. An *in vivo* model also limits the quick reproducibility of scans due the transient nature of the living model [33]. In the study outlined here, the backward facing step model was used because it allows for a more controlled experimental setup that can have the radio frequency coil placed just downstream of the backward facing step. The model also allows for the cessation of fluid flow to allow additional time to scan the resulting thrombus.

1.5 Computational Fluid Dynamics Modeling

Computational fluid dynamics (CFD) has become a valuable research tool that uses computers to solve the complex differential equations that describe fluid flow [34]. A CFD simulation requires preprocessing information on the fluid properties and geometry to be modeled [2, 34]. The geometry of the domain is represented by a mesh of discrete cells. In two dimensions, these cells represent finite areas, while in three dimensions the mesh cells represent finite volumes. The accuracy and validity of the solutions of a simulation depend on the geometry being adequately represented by the mesh [2]. A mesh that is comprised of too few cells will not represent the fluid flow correctly while a mesh that is comprised of too many cells becomes impractical to use due to the amount of computational power and time required to solve the associated equations [2]. Optimization of mesh geometry is important to obtain accurate solutions without adding unnecessary computations.

The actual CFD simulation is the systematic solving of the Navier-Stokes

Equations in relation to the fluid domain and conditions by computer algorithms. Initial conditions are required to define the pressure and velocity fields that exist at the start of a simulation [34]. Boundary conditions are also defined to describe the interaction between the fluid and the surfaces. The growing availability of high power supercomputers has made CFD simulations of complex geometries possible.

CFD post processing is the analysis of the solutions from the simulation to determine the pressure and velocity fields over the flow domain. This information is often conveyed with stream line and velocity vector plots for quick visual interpretation.

Chapter 2

This study will create the foundation for full CFD simulations of blood flow over a forming and formed thrombus which will occur at a later time. The experimental observation of thrombus formation with MRI will be used to create the geometries or meshes that are required for these later CFD simulations. This work and later efforts will improve the understanding of thrombus formation and the design considerations for cardiovascular assist devices.

Advances in biomedical and cardiac devices have facilitated this need for a better understanding of thrombosis and thromboembolization. A major concern for implantation of these devices is the development of thrombi and potential subsequent embolization. While the use of anticoagulants can reduce this risk of embolization, anticoagulant use has limitations and side effects [12]. Design considerations for cardiovascular devices include investigations of regions of flow separation. The process of thrombus formation is complicated by the changes in flow separation depending on the frequency and velocity of the flow [35]. The fluid mechanics, including flow separation, is one of the three factors that influence thrombosis as described by Virchow's triad [15, 16]. In this study the other two components of Virchow's triad, blood composition and the material interaction between the blood and the blood vessel wall or artificial wall, are not explicitly examined but their influence is noted. The information gained from this project should help improve the understanding of thrombosis and lead to the design of biomedical devices that are less prone to thrombi formation and embolization.

2.1 Design and Set up

To simulate the flow separation and subsequent thrombus formation developed in cardiovascular devices, a backward facing step was used. The model was made of two

acrylic segments each 200 mm in length that were connected at the backward facing step (Figure 2-1). The length of the upstream section of the model was selected to ensure fully developed flow over the step. The length of the downstream section was made 200 mm to guarantee the capture of the entire formed thrombus in the model. The model used a cylindrical channel that is 10 mm in diameter. The backward facing step was created by having a rise in the bottom of the channel from the inlet of the model towards the seam, at which point the acrylic occludes 2.5 mm of the channel bottom. This gradual change in geometry and development of the step was incorporated to minimize turbulence and blood damage in the fluid flow that would be caused by a rapid change in geometry.

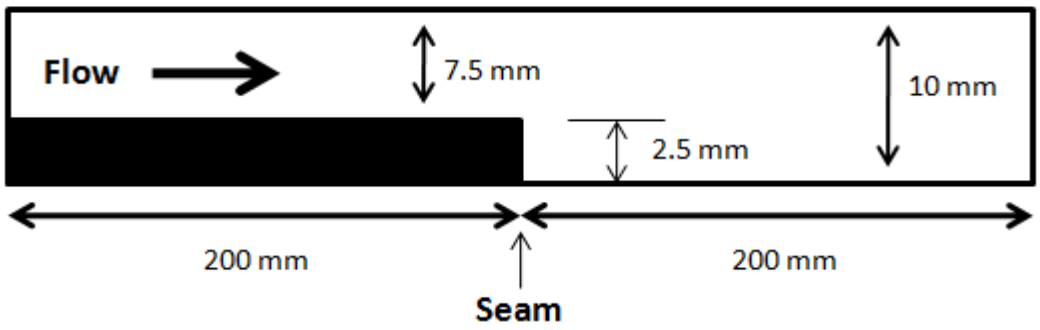

Figure 2-1: Experimental model

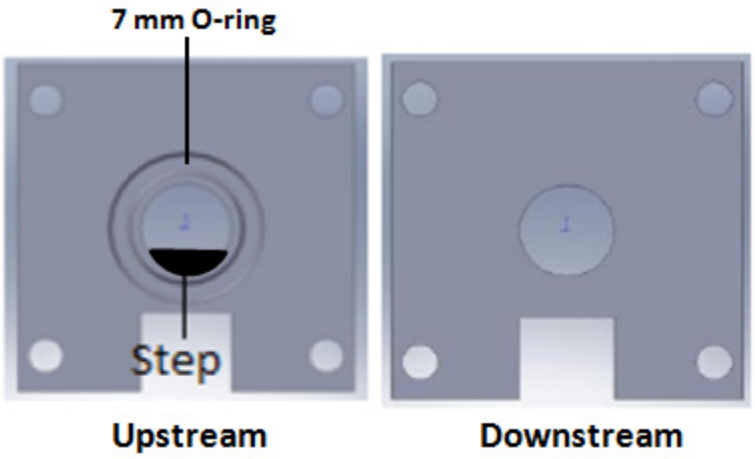

Figure 2-2: Close up of model step

To integrate the backward facing step model into a flow loop, 15.875 mm diameter inlet and outlet ports on the acrylic model allowed for plastic adapters to be attached that mated the 6.35 mm diameter plastic flow loop tubing to the model. The flow loop also included two plastic 6.35 mm Y adapters that allowed access to the loop for quick filling and draining of the loop. The 6.35 mm tubing was used to minimize total flow loop volume while maintaining a reasonable flow rate.

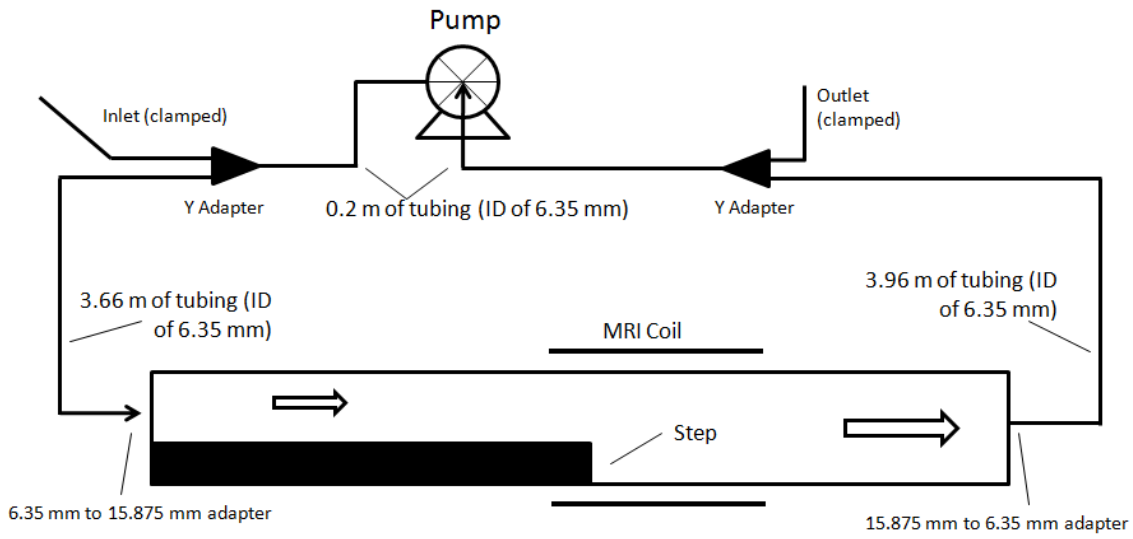

Figure 2-3: Diagram of flow loop.

The flow loop used approximately 8.2 meters of 6.35 mm tubing which allowed the model to be placed in the MRI while keeping the pump outside the magnetic field of the MRI. Total flow loop volume for the model was approximately 400 mL. A peristaltic pump (Masterflex, Cole-Palmer Instrument Company, Model No. 7520-40) was used to produce the flow. The waveform of the generated flow from the peristaltic pump is a symmetric continuous waveform similar to a sine wave. This does create a pulsatile flow but does not represent the more complex flow waveform found in normal systemic circulation.

To gather MRI data, the model was first assembled by placing a 7 mm rubber o-

ring between the two acrylic segments of the backward facing step and tightening the connection using four nylon nuts and bolts. Attached to the upstream end of the acrylic model was a 3.66 meter segment of tubing and attached to the downstream end of the acrylic model was a 3.96 meter segment of plastic tubing. These two tubing segments were connected with two plastic Y adapters to a small 0.2 meter tubing segment. This small tubing segment was then passed through the peristaltic pump and was used to generate the fluid flow in the loop. On the other end of the plastic Y adapters, two small 0.5 meter tubing segments were connected. These 0.5 meter tubing segments allowed for easier filling and draining of the flow loop. These inlet and outlet segments were clamped with hemostats when the loop was not being filled or drained.

2.2 Loop Operations

To assure that the model was free from contaminants, the flow loop and model were washed first with water and then with a phosphate buffered saline to create a biologically relevant 7.4 pH environment. This step ensured that any small amount of material or dust that may have accumulated in the flow loop since its last use was removed. Bovine blood was used in the flow loop. This bovine blood was obtained from the Pennsylvania State University Dairy Farm (IACUC #31075) within 18 hours prior to the experiments. Each 450 mL blood sample was extracted from the jugular vein using a 16 gauge needle and was collected into a blood donor bag that contained 63 mL of citrate phosphate dextrose anticoagulant solution. This blood bag was refrigerated in the time between collection and running the flow loop.

A 750 mL beaker was first rinsed with water and then phosphate buffered saline. Blood from the donor blood bag was then drained into a graduated cylinder for a 400 mL volume. This volume was then transferred into the 750 mL beaker to facilitate easy

preparation and filling of the blood for the flow loop. To prepare the blood for use in the flow loop, the anticoagulation effects of the citrate phosphate dextrose were reversed by adding 22 μL of 6% by mass of aqueous calcium chloride solution per mL of bovine blood. This process was performed immediately before filling the flow loop with blood to prevent clotting of the blood in the preparation beaker. Preparation and filling of the flow loop were both accomplished in under 5 minutes.

The entire loop and model was then washed with water and filled with phosphate buffered saline. To prepare the model for placement in the 7 Tesla Varian MRI scanner (Varian, Inc.), the downstream return tubing segment was taped to the upper corner of the model.

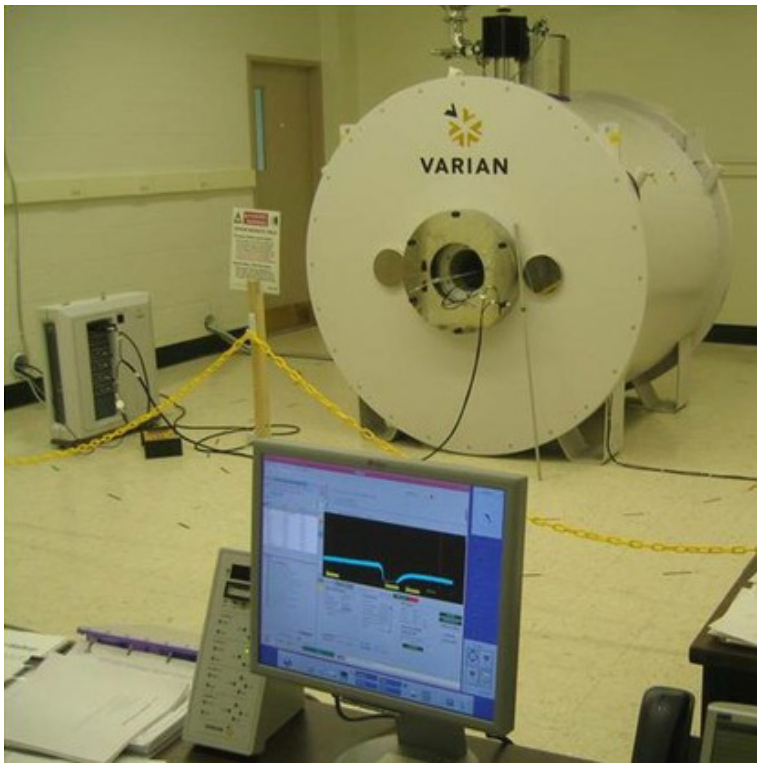

Figure 2-4: Picture of the 7T Varian MRI used for these experiments.

The entire model was placed in the radio frequency coil. The model was leveled in the RF coil in all three directions using a small 0.3 meter level. The model and radio frequency coil were then inserted 13 cm into the MRI for imaging. The recalcified bovine

blood was added to the loop, by displacing the phosphate buffered saline. The flow loop was then run for the desired time of 15, 30, 45, or 60 minutes at one flow rate. At the conclusion of the desired time period, the blood slowly displaced with the phosphate buffered saline. The displacement of the blood in the flow loop was performed to enhance the contrast between the thrombus and the fluid in the model. Three-dimensional magnetic resonance imaging of the thrombus that formed downstream of the backward facing step was conducted.

A tunable cylindrical radio frequency coil was used. This coil was tuned to 300 MHz and 50 Ohms in the MRI before imaging. Shimming was performed after the model was inserted into the MRI to create homogenous magnetic fields around the model. Three-dimensional MRI imaging was performed using a gradient field echo sequence. The final resolution of the three-dimensional image was 100 μm per pixel. This data was collected in an array sized 330x75x100 (ROxPE1xPE2) over an area from just upstream of the step to 5 cm downstream of the step. The total time of MRI imaging was 15 minutes and was determined from a time study. The details of this time study are in section 3. After performing several three-dimensional images, a flip angle of 15° was determined to give the highest contrast for imaging with a response time of 30 ms and echo time of 10 ms. The three-dimensional imaging sequence also utilized four averages of the thrombus to increase the signal-to-noise ratio. These parameters were chosen after studying the various factors impacting MRI imaging and the thrombus as described below in section 2.4. The image processing of the MRI data sets was extensive and is described in section 2.5.

2.3 Flow Rate Calibration

To set the peristaltic pump to provide the appropriate flow rate (0.79 L/min), bovine blood was pumped through the loop and collected into a graduated cylinder for 15 seconds. This flow rate was chosen to mimic the flow rate typically provided by an adult heart at 75bpm. This calibration takes into account any effects that may reduce the flow rate in the flow loop when using blood as opposed to water. This was done only once for the flow loop model during the study and not every time the flow loop was used experimentally.

2.4 Thrombus Imaging Studies

Before data could be collected, the amount of time that the formed thrombus maintained its structure had to be determined. The resolution and signal-to-noise ratio of the MRI data improves with a longer imaging time and averaging of multiple MRI data sets. This increase in resolution must be balanced with degradation of the thrombus over time. These changes are the result of the thrombus beginning to dissolve into the PBS that replaces the blood during imaging. To determine the time period during which the thrombus is intact, a study was performed where the loop was run for 35 minutes at a flow rate 0.79 L/min. The blood in the loop was then replaced with PBS and three-dimensional imaging was performed. This imaging of the thrombus was then repeated every 15 minutes for 3 hours and 15 minutes to observe the degradation of the thrombus.

The collected data was then analyzed to determine the changes in thrombus structure over the three hour imaging period. After considering the changes in size of the thrombus and weighing the benefits of imaging time for resolution, a maximum time of 15 minutes was selected. The full data, discussion, and analysis of this process can be found in section 3.1.

2.5 MRI Image Data Processing

Post processing of the MRI data was conducted to construct a three-dimensional mesh of the thrombus. The initial MRI data was encoded by the MRI software in a proprietary format used by the Varian Corporation. To extract the data, a MATLAB code was obtained from the Pennsylvania State University's Huck Institutes Magnetic Resonance Center. This code was modified to extract and compile 660 bitmap image files for each three-dimensional data set using MATLAB (MathWorks, Inc.). It was important to ensure during this step that the code was modified for each three-dimensional data set. These modifications changed the scale of the signal intensity to be better represented by the 255 levels of intensity present in the bitmap file format. Small changes in model alignment were also corrected in the code. Each data set's signal intensity and exact position in the MRI varied a small but significant amount when accounting for the 100 micron scale resolution.

These 660 bitmap files were then image processed in AVIZO (Visualization Sciences Group SAS). This program allowed for the identification and isolation of the model and thrombus from the MRI images. It was then able to combine all 660 bitmap files per data set into a three-dimensional representation. From this three-dimensional representation, the volume of the isolated thrombus was calculated through AVIZO. Some amount of error was present in the calculation of thrombus volume and was related to noise and artifacts present in the MRI data. While the precision of the calculated volume is not high, the trends in volume are quite relevant. This volume information was used to compare the sizes of the formed thrombi.

Most importantly, AVIZO generated a surface mesh of the three-dimensional model and thrombus. This mesh ranged from approximately 625,000 to 725,000

unstructured triangular surfaces for all of the imaging data sets. This was then converted into a stereolithography file that could be further processed for use by the OpenFOAM CFD solvers (OpenCFD, INC.).

Due to the constraints of the MRI, the area imaged was limited to only the area from the backward facing step to approximately 5 cm downstream of the step. The open downstream and upstream portions of the model were extended to fully represent the model and fluid flow using the Rhinoceros computer aided design software package, which also has the important capability of easily importing and exporting stereolithography files. Hence, each stereolithography file from AVIZO was imported to Rhinoceros for upstream and downstream extension.

After extension, each file was then smoothed and cleaned via MeshLab (ISTI-CNR). MeshLab is an open source three-dimensional mesh processing software that employs several different algorithms to remove noise in unstructured meshes. This manipulation was done to remove artifacts from the MRI imaging process in the stereolithography files. The amount of smoothing applied was intentionally minimal as not to remove detail from the formed thrombi.

2.6 Mesh Generation

To convert the cleaned and extended stereolithography file from MeshLab into a usable mesh format for CFD studies using the OpenFOAM software package, the snappyHexMesh utility in OpenFOAM was used. This converted the triangular stereolithography mesh into a three-dimensional hexahedral mesh that can be used by OpenFOAM in CFD studies. The snappyHexMesh utility was performed using Pennsylvania State University's High Performance Computing clusters. The resulting meshes had the geometry of the backward facing step and integrated thrombus with a

total cell number between 900,000 and 1 million cells. These completed meshes were available for later CFD study.

Chapter 3

3.1 Thrombosis Imaging Time Study Results and Discussion

To ensure that the meshes generated by this study are faithful to the actual thrombus, a series of MRI images were taken to determine how much degradation of the thrombus occurred in the PBS. The thrombus was formed over 35 minutes of flow loop operation at a flow rate of 0.79 L/min. Further method information on the time study can be found in section 2.3.

After the MRI data for the time study was processed, a change in thrombus size was noted both qualitatively and quantitatively. Using image segmentation in AVIZO, the formed thrombus was isolated in each of the 13 time steps. Qualitatively, we observed that the thrombus size was reduced over the course of the time study (Figures 3-1 through 3-10).

To observe the changes in thrombus morphology, three cross sections were taken of the formed thrombus. One cross section was close to the backward facing step, one was approximately midway through the expected length range of the thrombus, and one was at the far end of the expected thrombus range. For comparison, these were defined as being at 4 mm, 14 mm, and 29 mm downstream of the end of the backward facing step. The cross sections for the time study can be found in Figures 3-11 through 3-15.

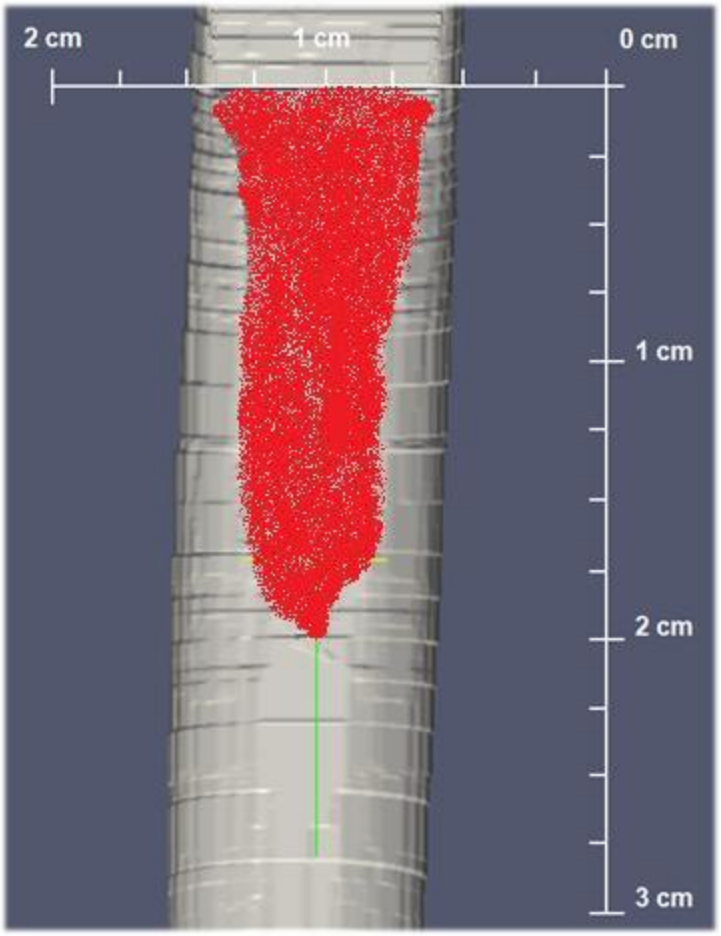

Figure 3-1: Top down view of the formed thrombus from MRI Data after 15 minutes in PBS.

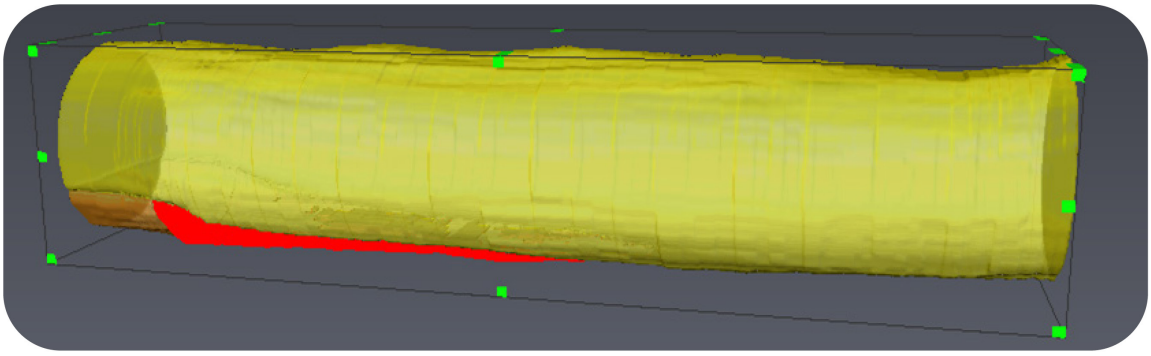

Figure 3-2: Image of the model showing the thrombus highlighted in red after 15 minutes in PBS.

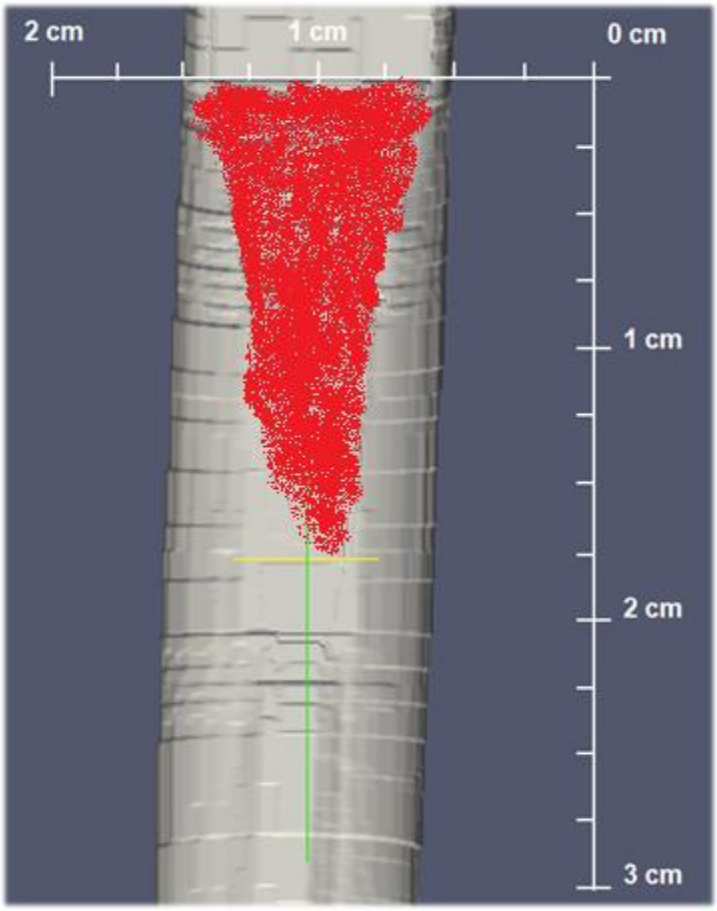

Figure 3-3: Top down view of the formed thrombus from MRI Data after 75 minutes in PBS.

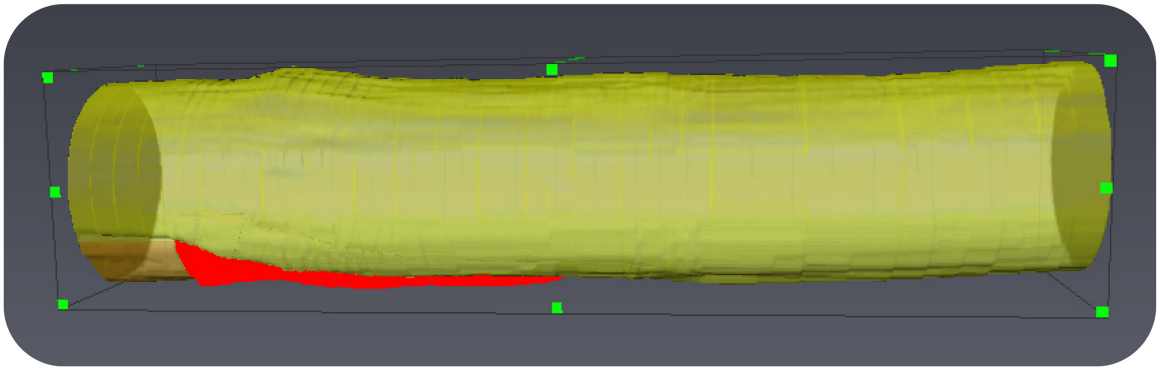

Figure 3-4: Image of the model showing the thrombus highlighted in red after 75 minutes in PBS.

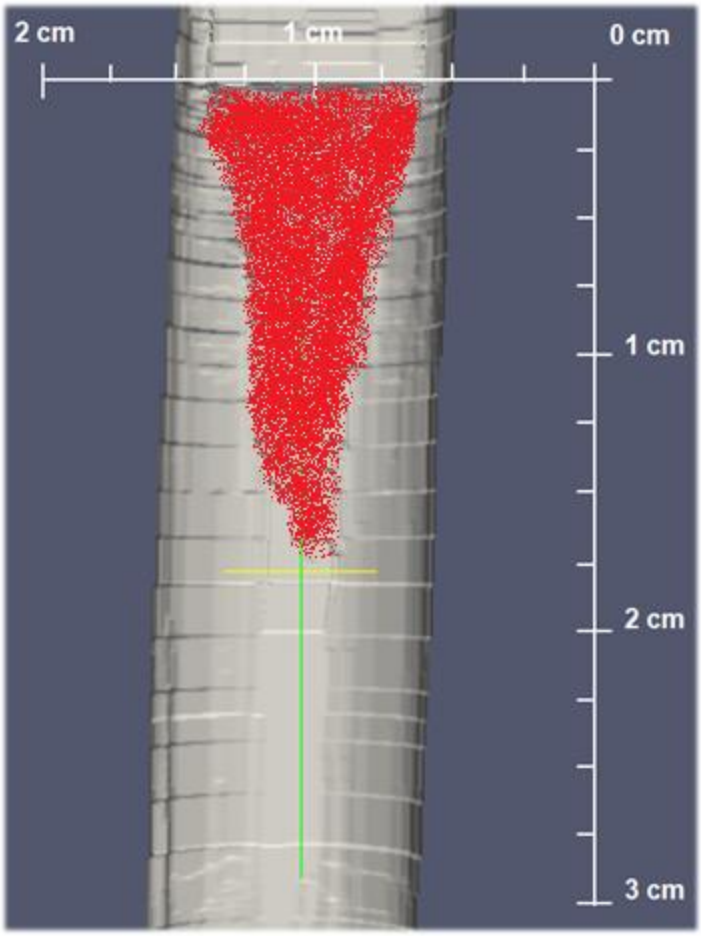

Figure 3-5: Top down view of the formed thrombus from MRI Data after 120 minutes in PBS.

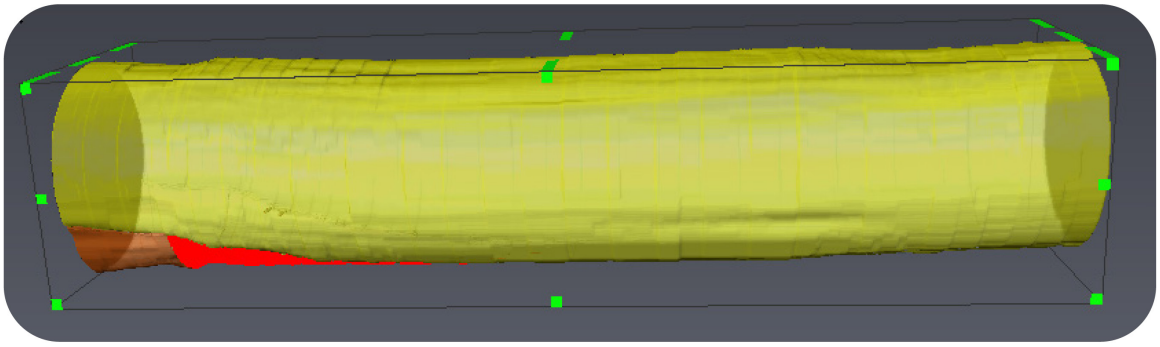

Figure 3-6: Image of the model showing the thrombus highlighted in red after 120 minutes in PBS.

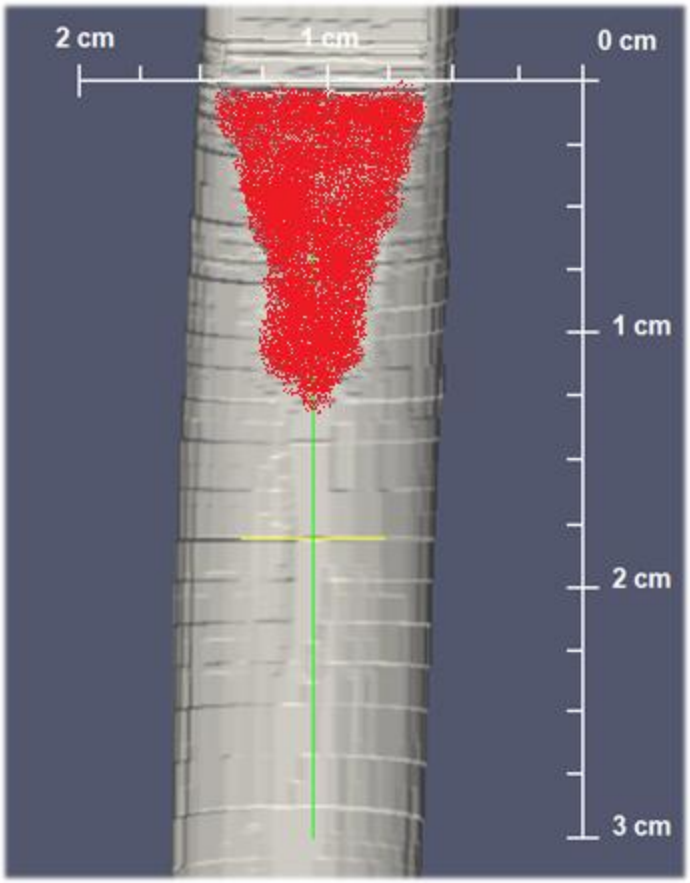

Figure 3-7: Top down view of the formed thrombus from MRI Data after 165 minutes in PBS.

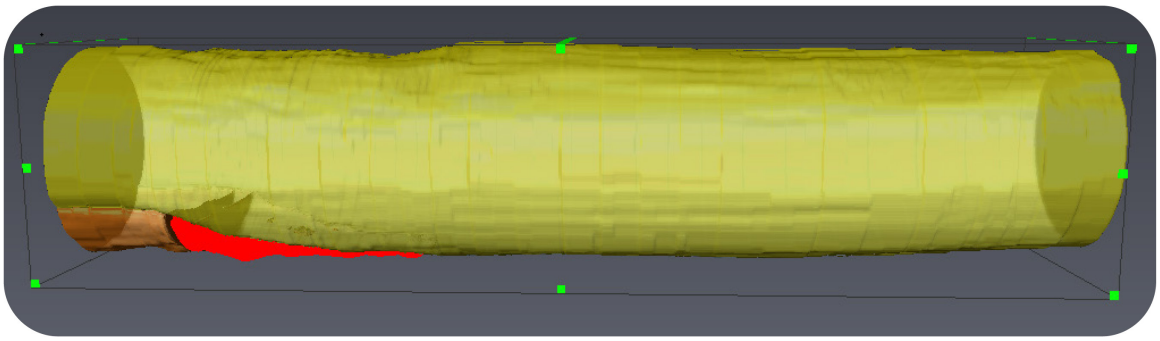

Figure 3-8: Image of the model showing the thrombus highlighted in red after 165 minutes in PBS.

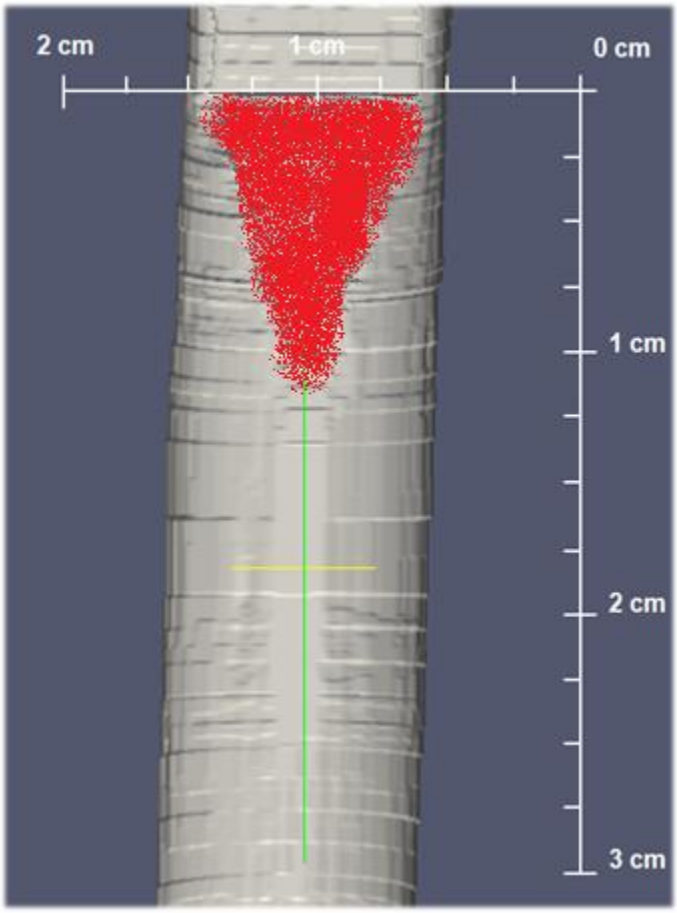

Figure 3-9: Top down view of the formed thrombus from MRI Data after 195 minutes in PBS.

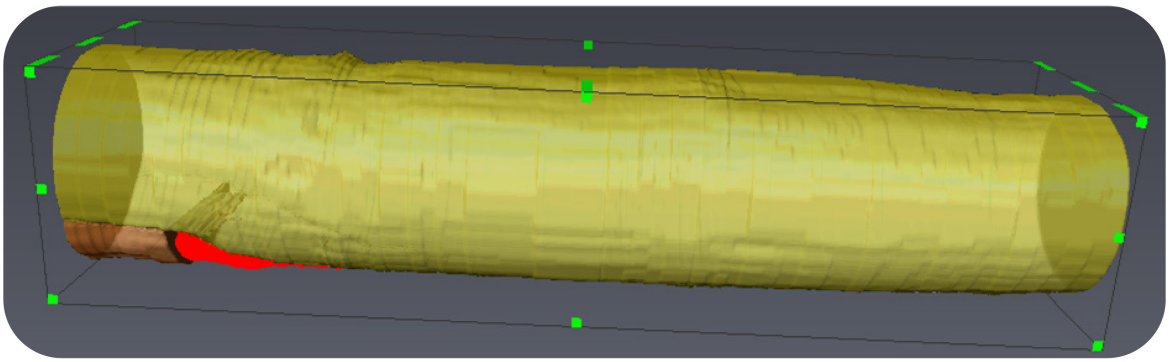

Figure 3-10: Image of the model showing the thrombus highlighted in red after 195 minutes in PBS.

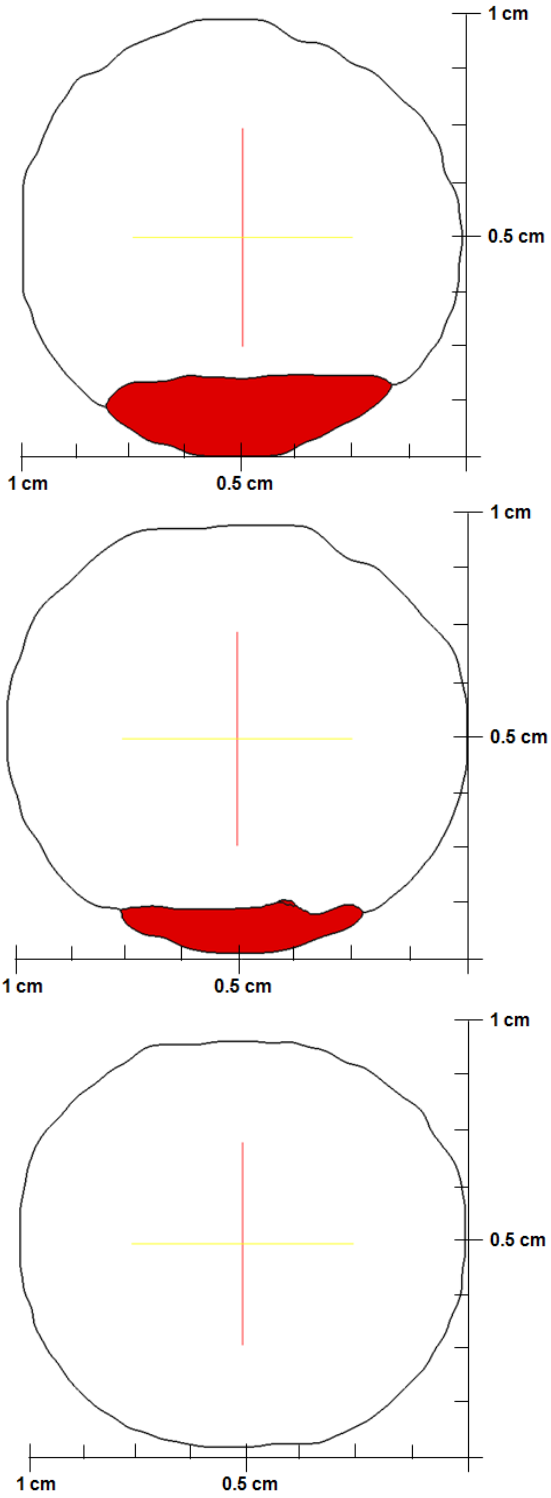

Figure 3-11: Cross sections of the channel and thrombus after 35 minutes of flow. The thrombus imaged after being in PBS for 15 minutes. The top, middle, and bottom image are at 4 mm, 14 mm, and 29 mm downstream of the backward facing step. The thrombus has been highlighted in red.

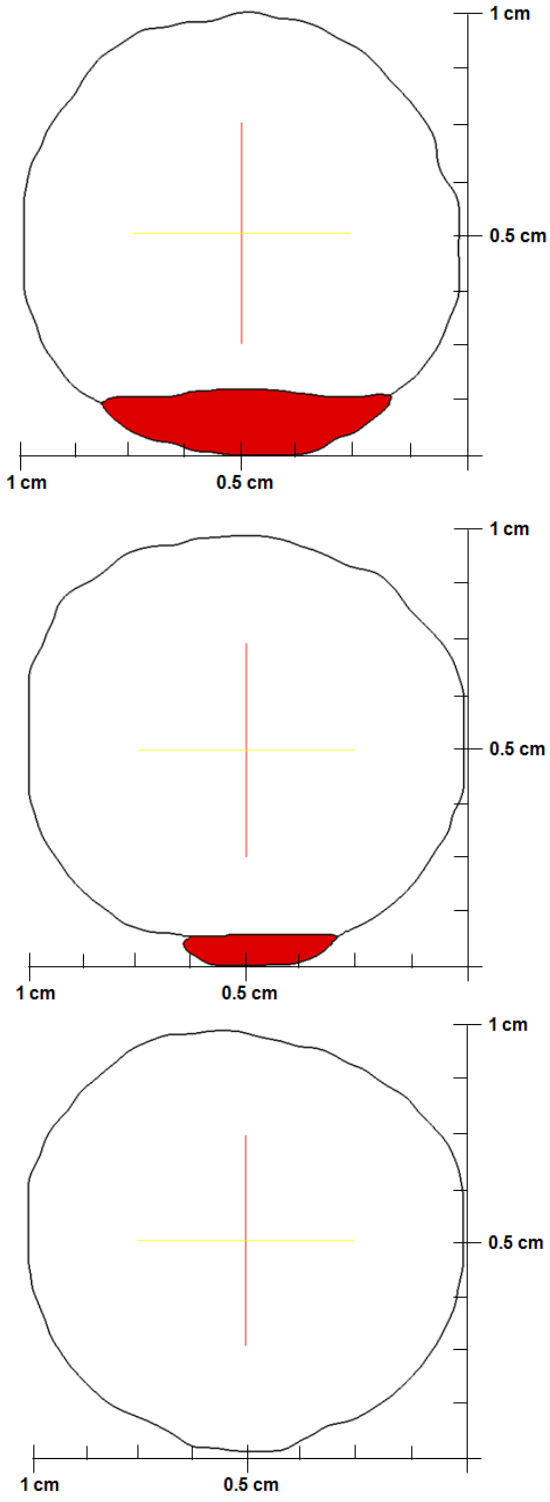

Figure 3-12: Cross sections of the channel and thrombus after 35 minutes of flow. The thrombus imaged after being in PBS for 75 minutes. The top, middle, and bottom image are at 4 mm, 14 mm, and 29 mm downstream of the backward facing step. The thrombus has been highlighted in red.

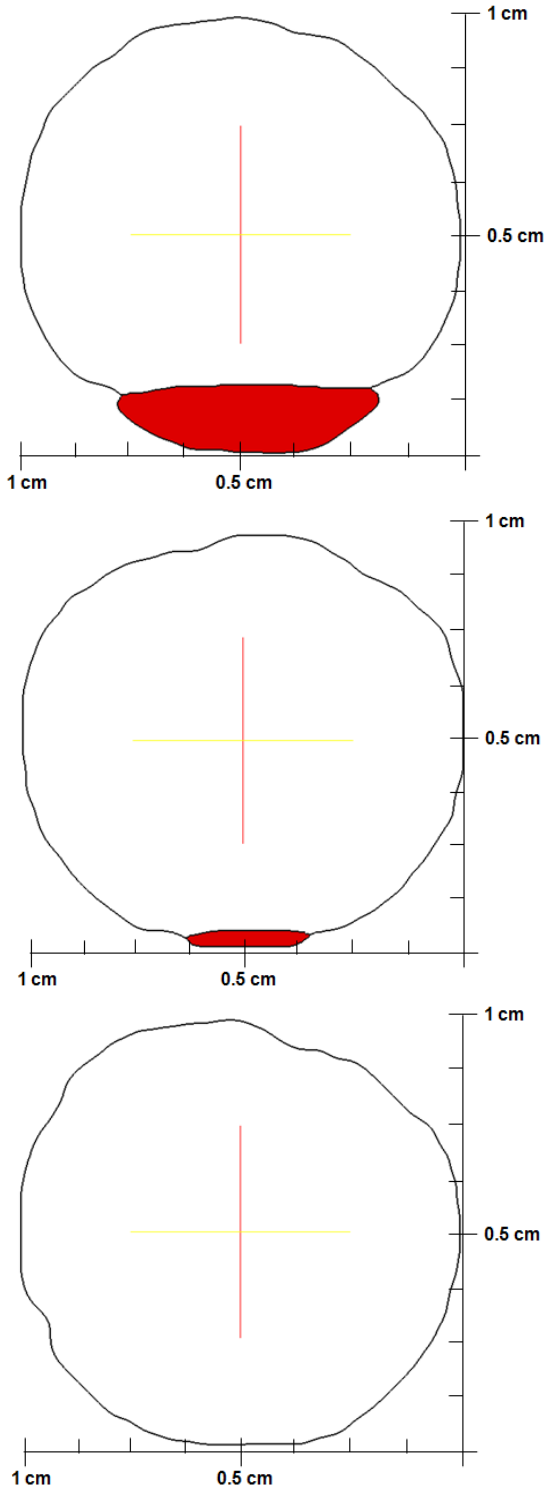

Figure 3-13: Cross sections of the channel and thrombus after 120 minutes of flow. The thrombus imaged after being in PBS for 15 minutes. The top, middle, and bottom image are at 4 mm, 14 mm, and 29 mm downstream of the backward facing step. The thrombus has been highlighted in red.

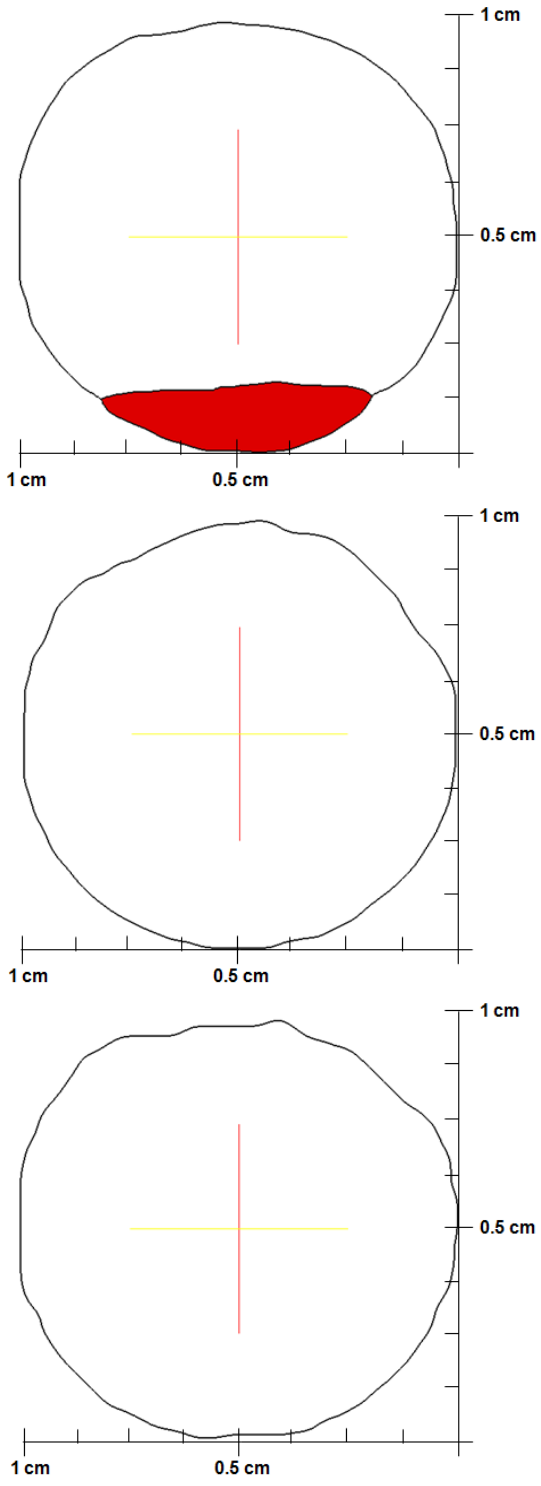

Figure 3-14: Cross sections of the channel and thrombus after 165 minutes of flow. The thrombus imaged after being in PBS for 15 minutes. The top, middle, and bottom image are at 4 mm, 14 mm, and 29 mm downstream of the backward facing step. The thrombus has been highlighted in red.

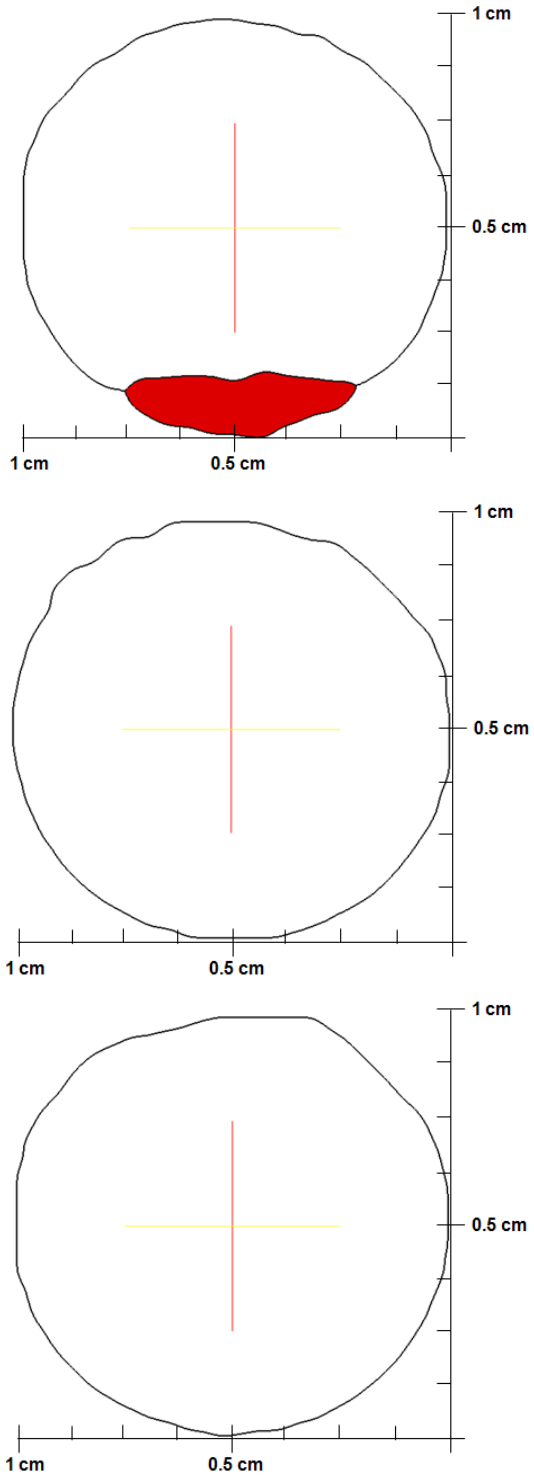

Figure 3-15: Cross sections of the channel and thrombus after 195 minutes of flow. The thrombus imaged after being in PBS for 15 minutes. The top, middle, and bottom image are at 4 mm, 14 mm, and 29 mm downstream of the backward facing step. The thrombus has been highlighted in red.

The side views and cross sections of the thrombus qualitatively show a reduction in thrombus size the longer the PBS is in place. To quantify this change in thrombus size, the volume of the thrombus was used. The volume of the thrombus for each time step was calculated with AVIZO. The volumes of the thrombus are listed below in Table 3-1.

Table 3-1: This table shows the change in thrombus volume over time. The Thrombus Volume Remaining is referenced to the calculated volume after 15 minutes.

Time the Thrombus was in PBS (min)	Volume of Thrombus (cc)	Thrombus Volume Remaining
15	0.1265	
30	0.1112	87.9%
45	0.1062	84.0%
60	0.0964	76.2%
75	0.0944	74.6%
90	0.0766	60.6%
105	0.0760	60.1%
120	0.0701	55.4%
135	0.0717	56.7%
150	0.0641	50.6%
165	0.0531	41.9%
180	0.0520	41.1%
195	0.0496	39.2%

To better observe the trends in the volume change, a graph (Figure 3-16) of this data was created comparing thrombus volume and the time the thrombus was in PBS for MRI imaging. The percent volume of thrombus remaining between the thrombus at 15 minutes and each subsequent time step was plotted in Figure 3-17.

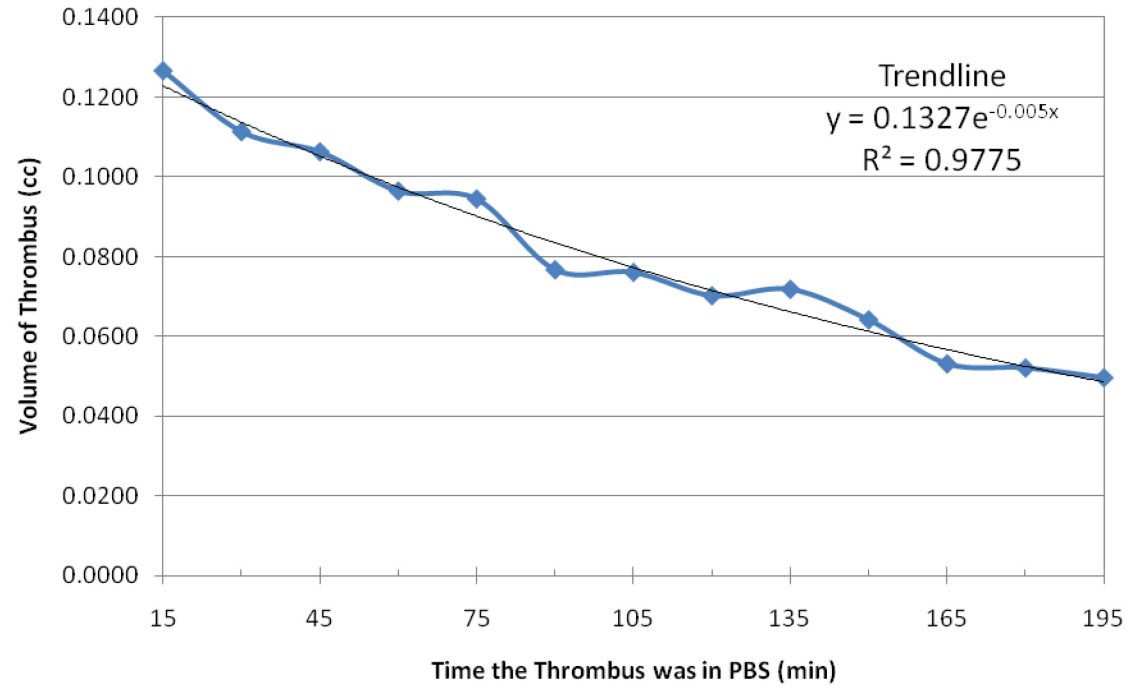

Figure 3-16: Graph illustrating the change in thrombus volume over the time it was in PBS. A curve was fit to the data using an exponential equation: $y = 0.1327e^{-0.05x}$, $R^2=0.9775$.

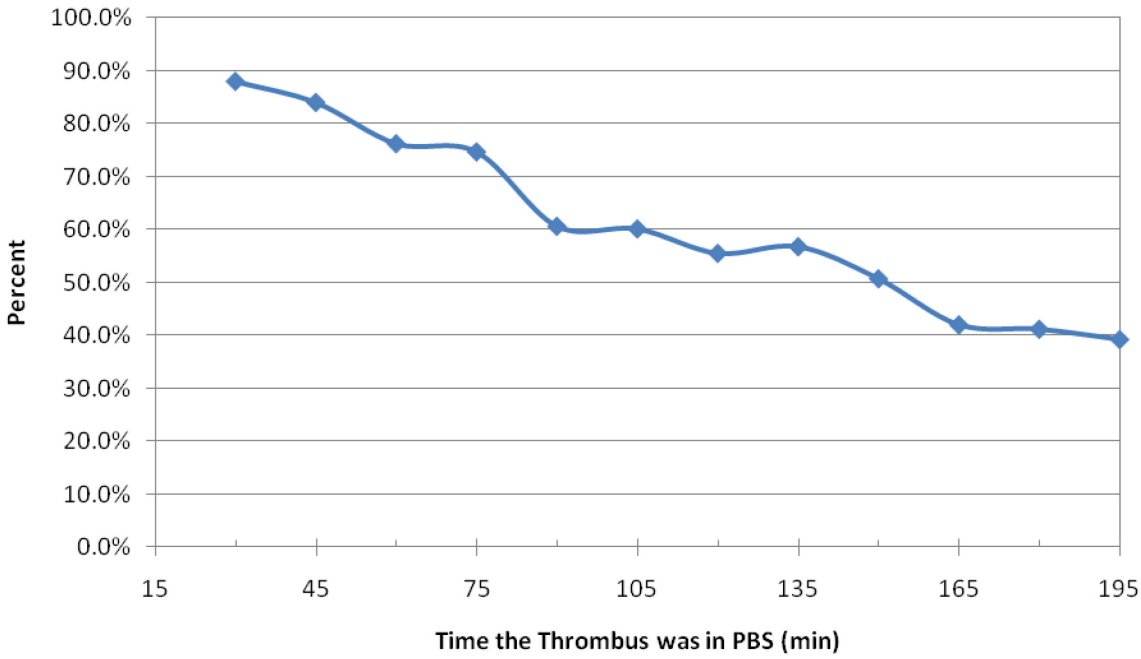

Figure 3-17: A graph illustrating the percentage remaining of volume between the formed thrombus at 15 minutes in PBS and the subsequent time steps.

Figure 3-16 clearly shows that thrombus degradation begins immediately when PBS is placed in the flow loop for MRI imaging. A curve was fit to the data in Figure 3-16 using an exponential equation: $y = 0.1327e^{-0.05x}$, $R^2=0.9775$. This exponential decay is likely related to the decreasing amount of exposed surface area in relation to volume slowing the degradation of the thrombus as time progresses. Figure 3-17 shows that there is a large percent change in volume of the thrombus after it is placed in PBS. To ensure the most accurate MRI images of the formed thrombus, the amount of time the PBS is in the flow loop should be minimized. To achieve acceptable MRI resolution and signal-to-noise ratios, the MRI acquisition must be at a minimum 15 minutes. Therefore, 15 minutes was determined to be the amount of time available for MRI imaging.

3.2 Thrombi Images Results and Discussion

Using the protocol described in the methods section, the flow loop and model were used to generate thrombi after the blood flow had run for 15 minutes, 30 minutes, 45 minutes, and 60 minutes. These thrombi were all formed at a flow rate at 0.79 L/min. The reconstructed MRI images of these thrombi are presented below in Figures 3-18 through 3-27. Figures 3-28 through 3-32 show the cross sections of the thrombus at 4 mm, 14 mm, and 29 mm downstream of the backward facing step.

Table 3-2 presents the experiment number of flow time and date.

Table 3-2: This table shows the date and flow rate of each experiment.

Exp #	Date	Flow Time
1	02/24/11	15 Minutes
2	02/03/11	30 Minutes
3	02/22/11	30 Minutes
4	03/03/11	45 Minutes
5	03/17/11	60 Minutes

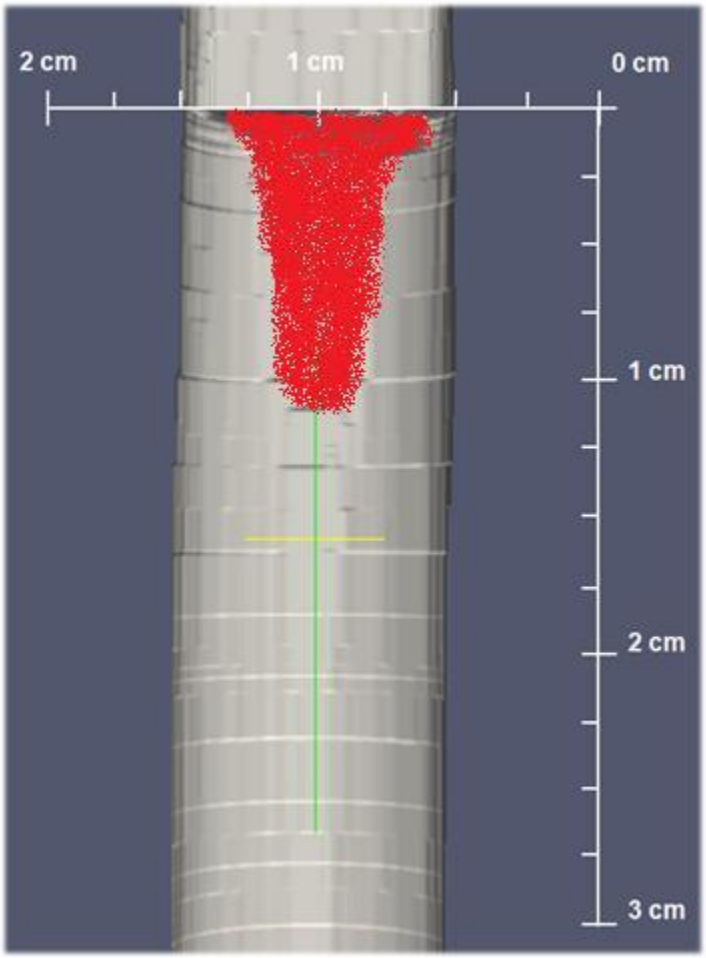

Figure 3- 18: Top down view of the formed thrombus from experiment # 1.

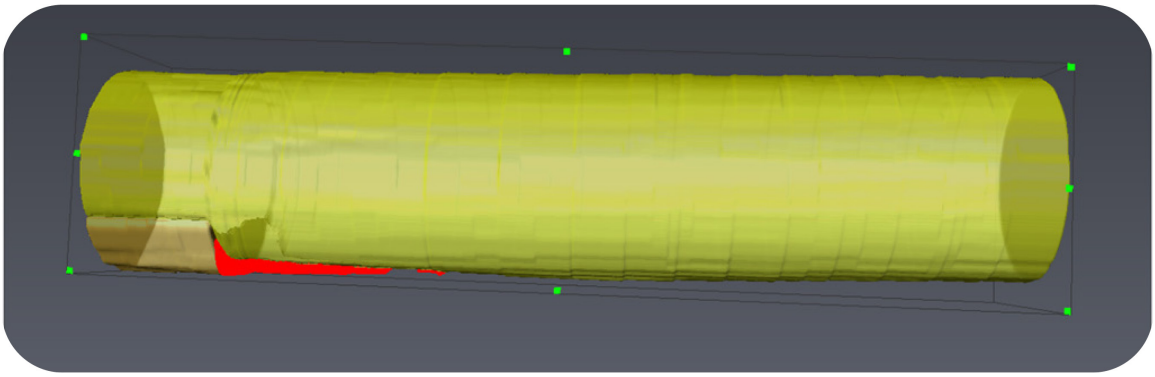

Figure 3-19: Image of the model showing the thrombus highlighted in red from experiment # 1.

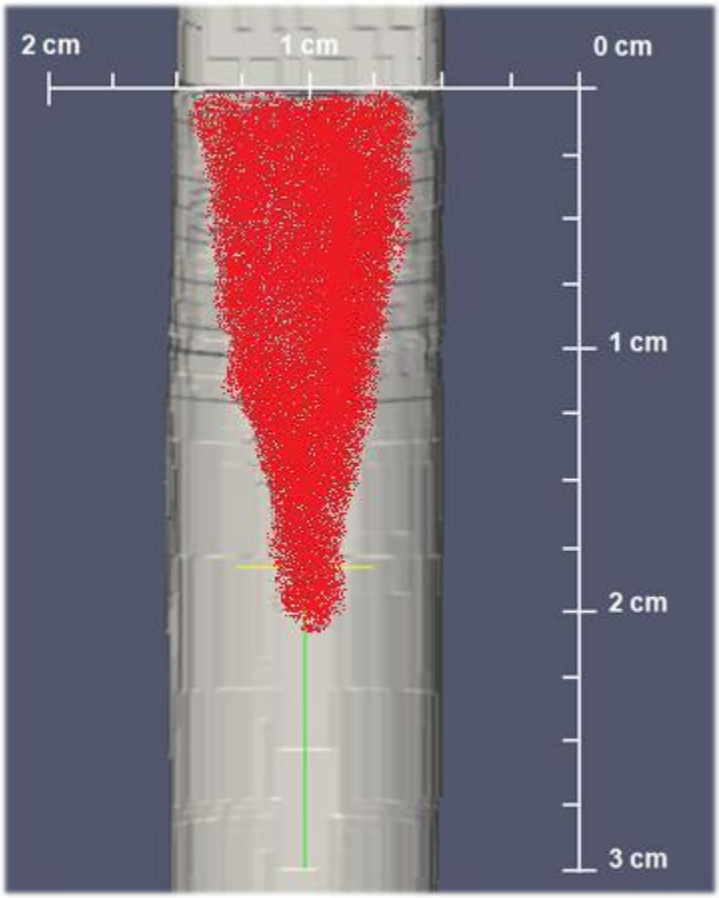

Figure 3- 20: Top down view of the formed thrombus from experiment #2.

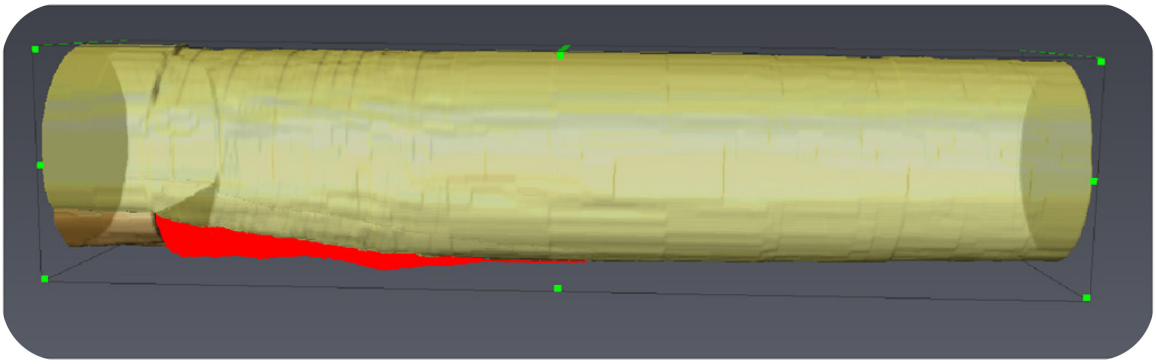

Figure 3-21: Image of the model showing the thrombus highlighted in red from experiment #2.

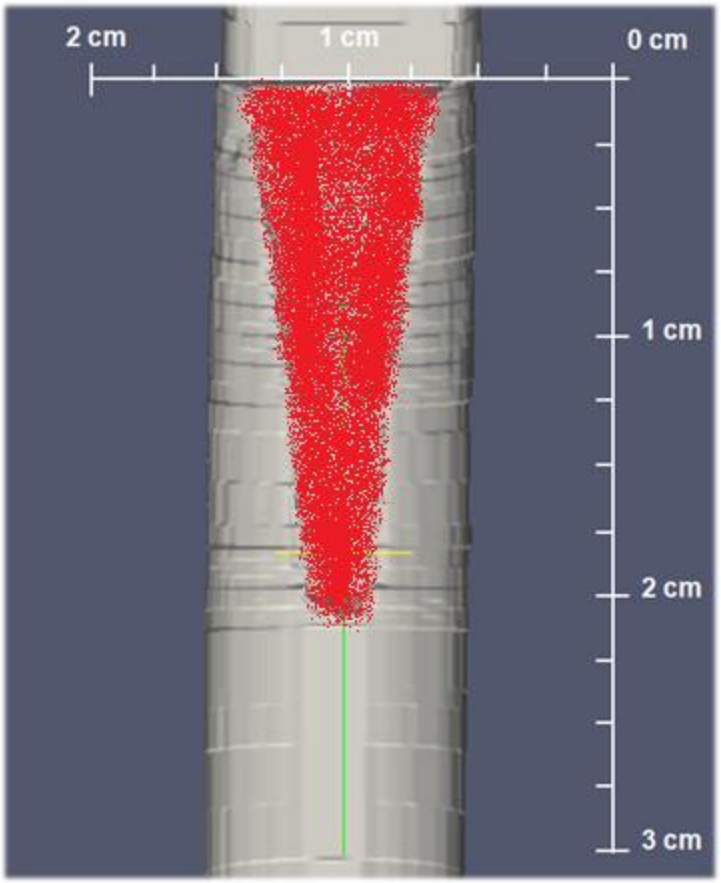

Figure 3- 22: Top down view of the formed thrombus from experiment #3.

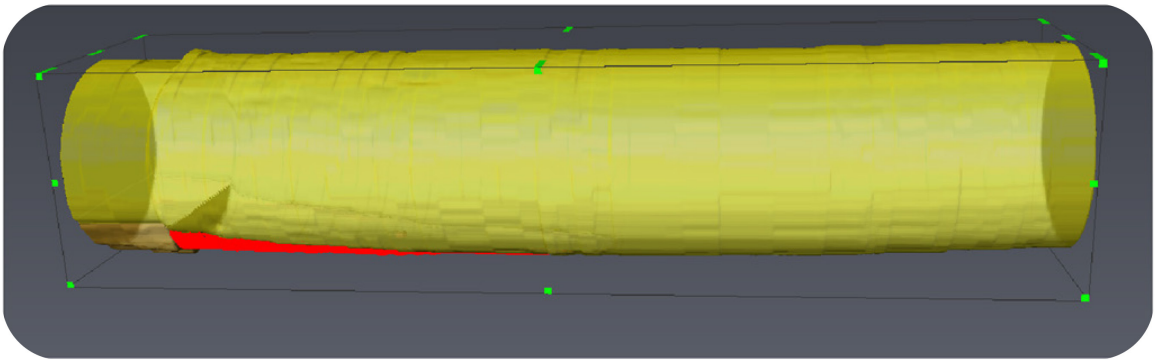

Figure 3-23: Image of the model showing the thrombus highlighted in red from experiment #3.

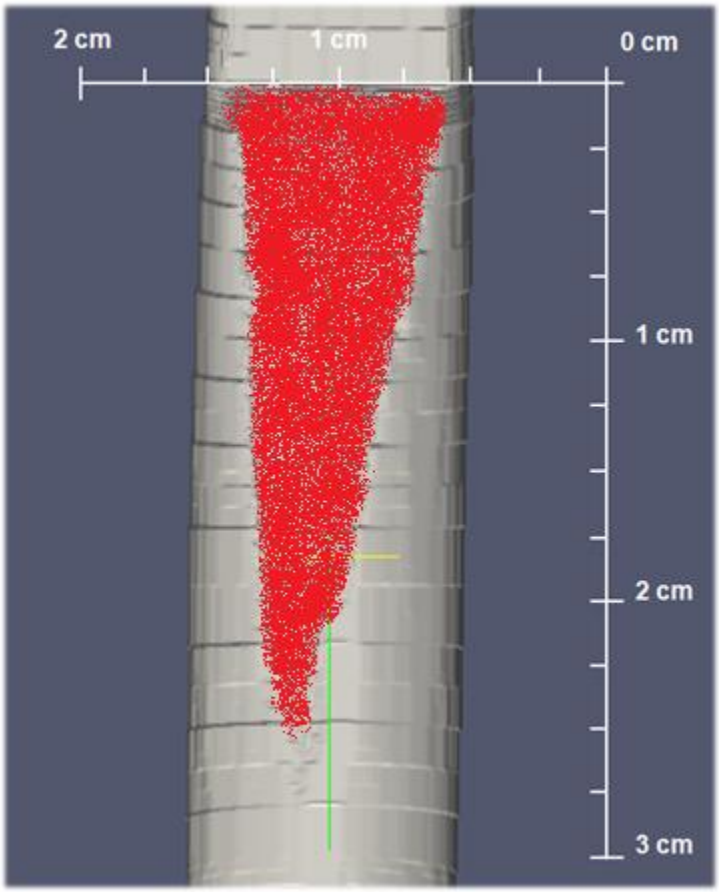

Figure 3-24: Top down view of the formed thrombus from experiment #4.

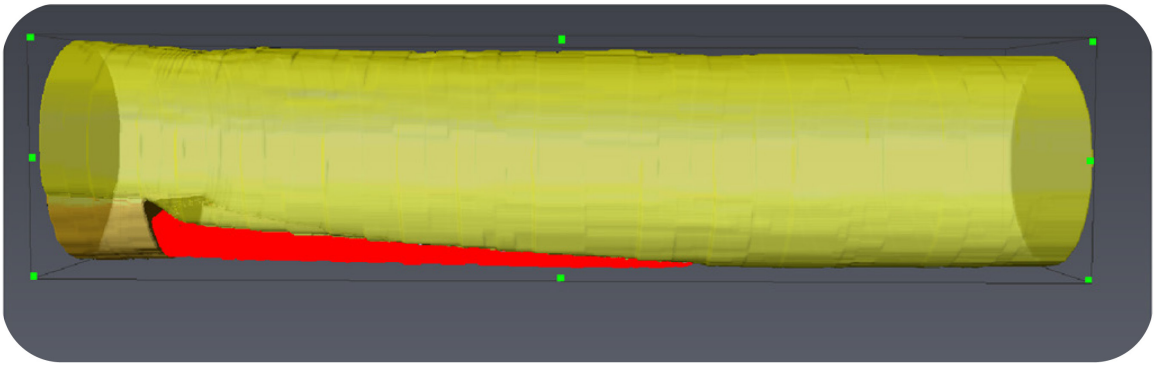

Figure 3-25: Image of the model showing the thrombus highlighted in red from experiment #4.

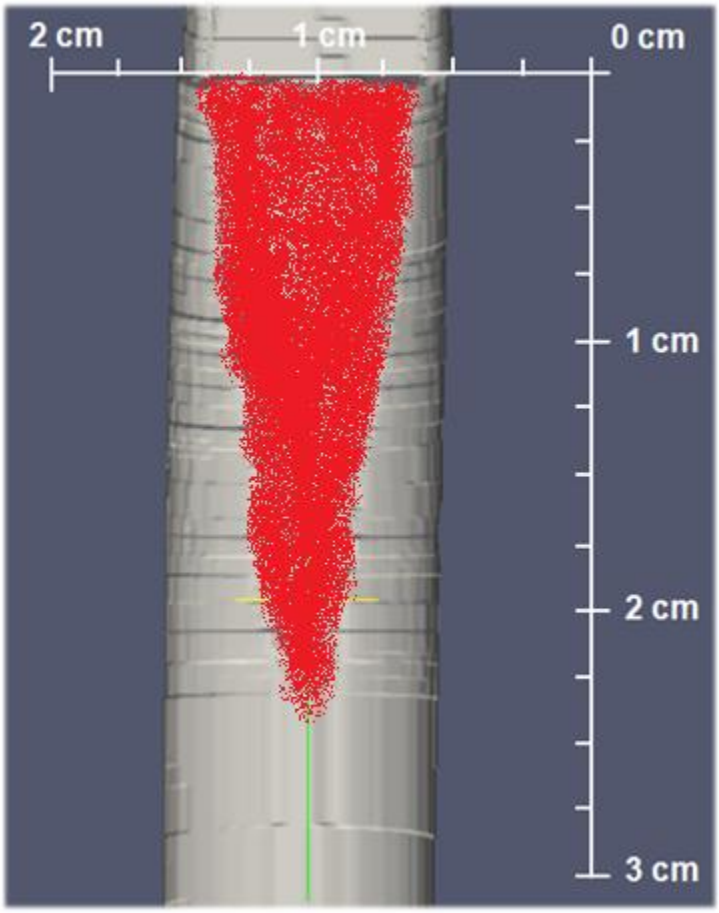

Figure 3-26: Top down view of the formed thrombus from experiment #5.

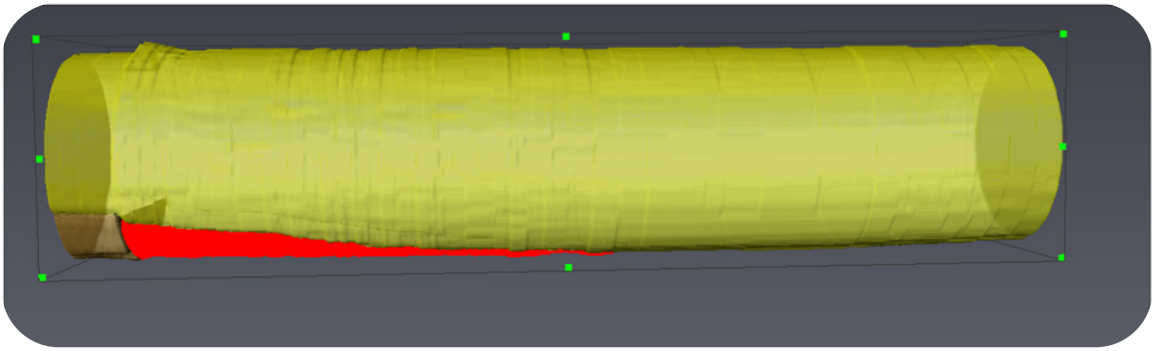

Figure 3-27: Image of the model showing the thrombus highlighted in red from experiment #5.

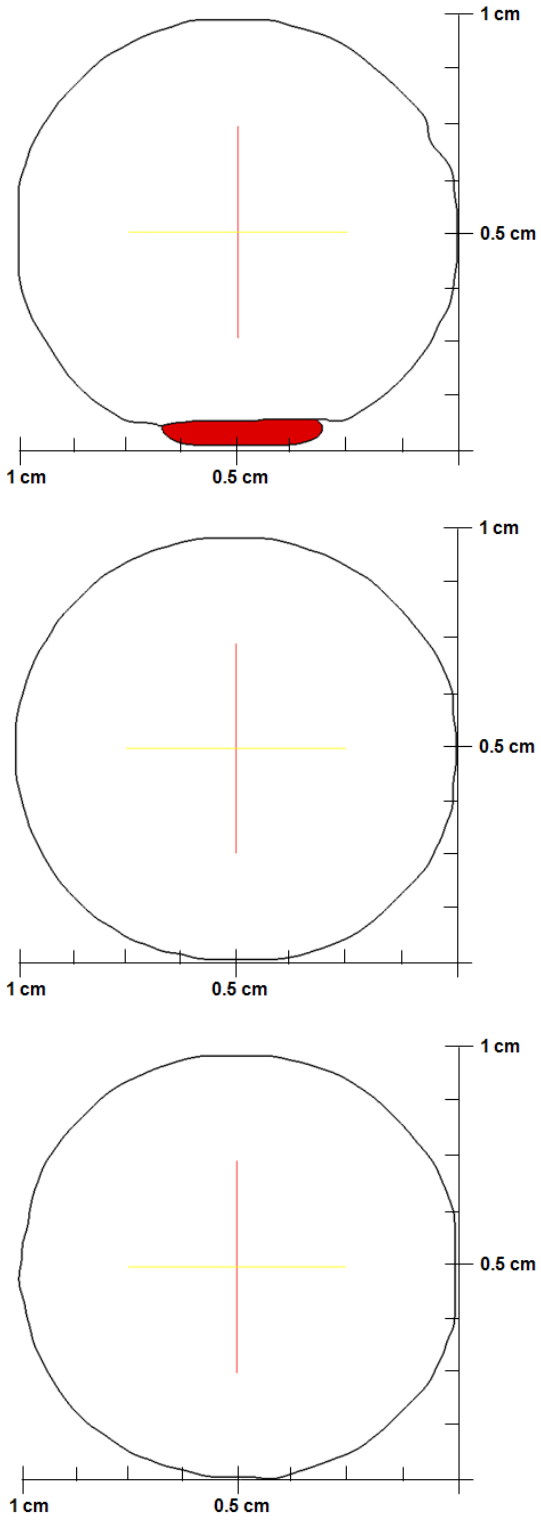

Figure 3-28: Cross sections of the channel and thrombus from experiment #1. The top, middle, and bottom image are at 4 mm, 14 mm, and 29 mm downstream of the backward facing step. The thrombus has been highlighted in red.

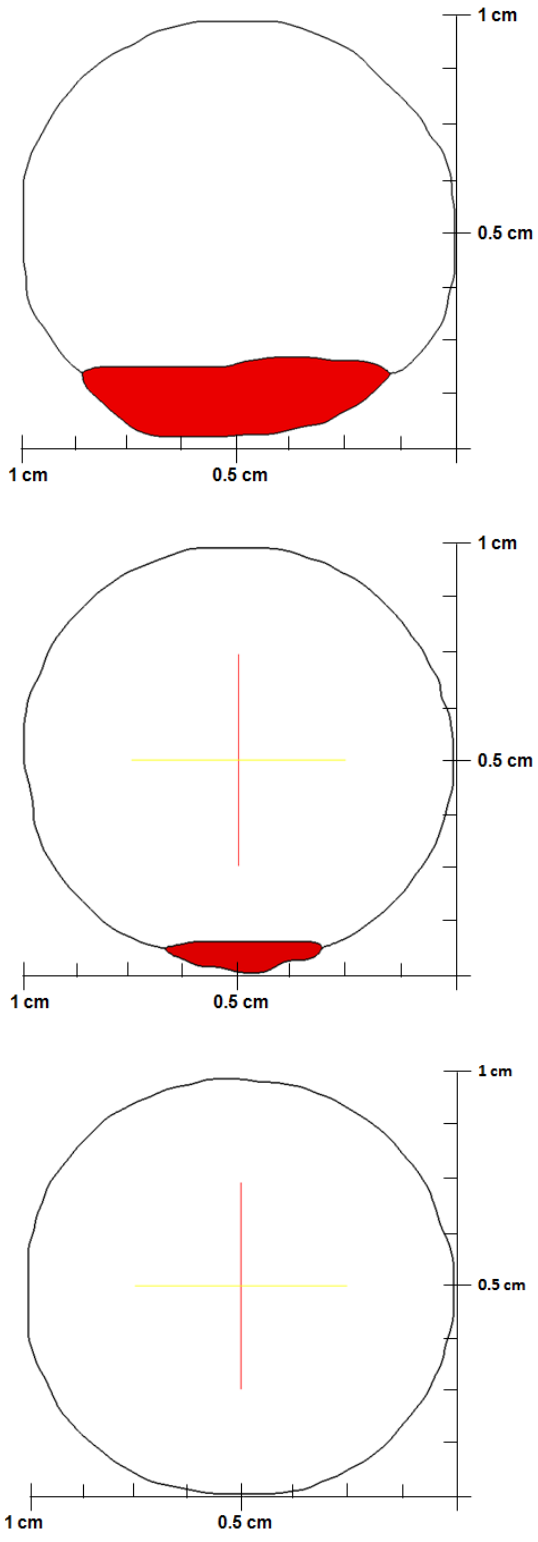

Figure 3-29: Cross sections of the channel and thrombus from experiment #2. The top, middle, and bottom image are at 4 mm, 14 mm, and 29 mm downstream of the backward facing step. The thrombus has been highlighted in red.

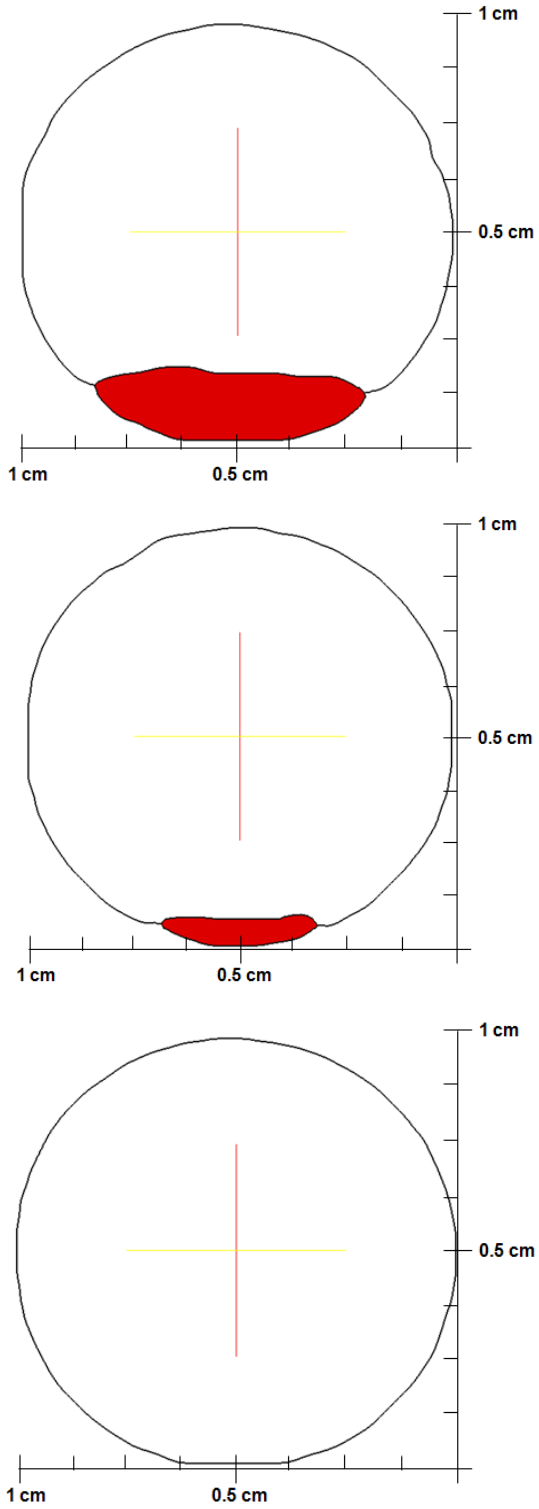

Figure 3-30: Cross sections of the channel and thrombus from experiment #3. The top, middle, and bottom image are at 4 mm, 14 mm, and 29 mm downstream of the backward facing step. The thrombus has been highlighted in red.

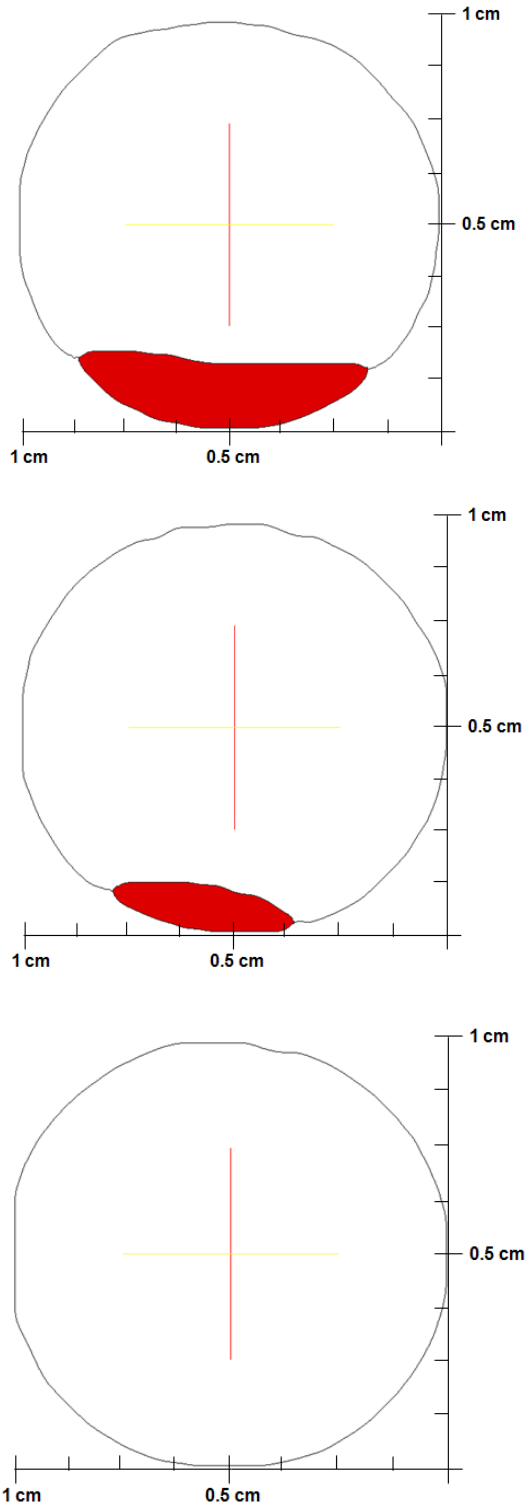

Figure 3-31: Cross sections of the channel and thrombus from experiment #4. The top, middle, and bottom image are at 4 mm, 14 mm, and 29 mm downstream of the backward facing step. The thrombus has been highlighted in red.

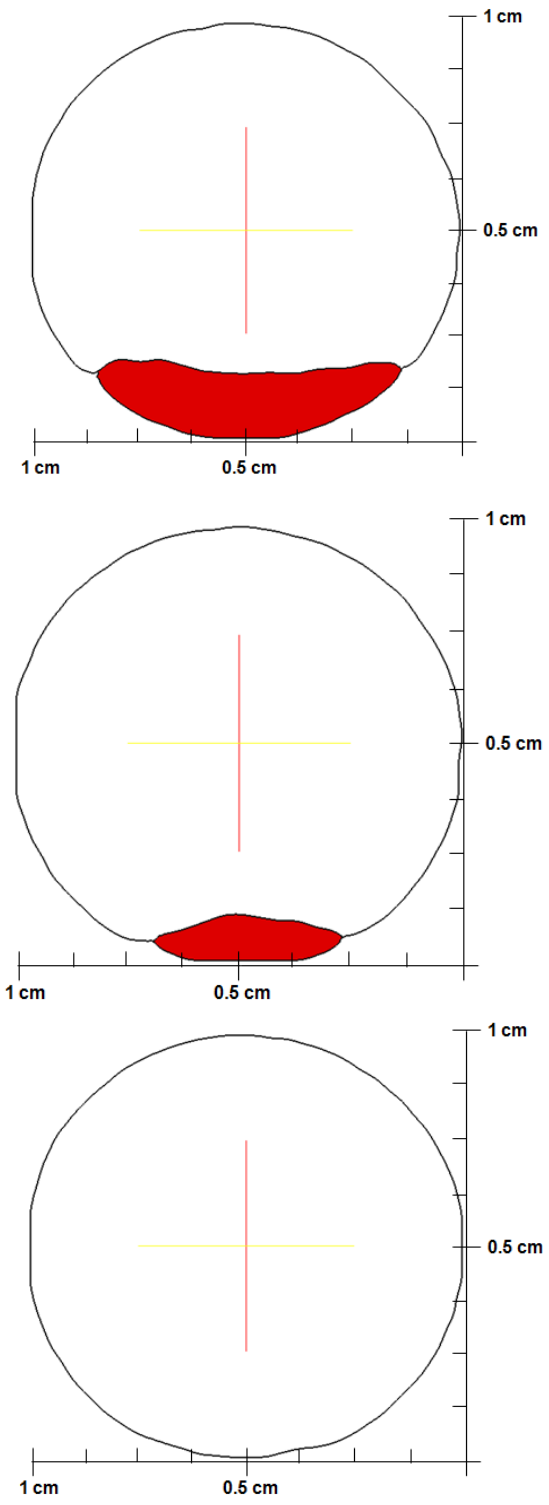

Figure 3-32: Cross sections of the channel and thrombus from experiment #5. The top, middle, and bottom image are at 4 mm, 14 mm, and 29 mm downstream of the backward facing step. The thrombus has been highlighted in red.

Figures 3-18 through 3-27 present the side and top view of the formed thrombi at 15, 30, 45, and 60 minutes. Cross section Figures 3-28 through 3-32 show that the thrombi are increasing in size at each position as the time of blood flow increases.

Comparing Figures 3-29 and 3-30, both of which were formed after 30 minutes of flow, the shapes of the thrombi are different. The general dimension of the formed thrombus in figures 3-29 and 3-30 are similar, the morphology is not exactly the same. This indicates that thrombus formation is not identical across experiments even using the same parameters.

Below Table 3-3 shows the calculated volume of the formed thrombus in each experiment.

Table 3-3: This table shows the date and flow time of the each of the experiments. The volume of the formed thrombus in each experiment was calculated with AVIZO.

Exp #	Date	Flow Time	Volume (cc)
1	02/24/11	15 Minutes	0.024
2	02/03/11	30 Minutes	0.114
3	02/22/11	30 Minutes	0.103
4	03/03/11	45 Minutes	0.124
5	03/17/11	60 Minutes	0.131

To better see the trends in thrombus volume in relation to minutes of blood flow, the thrombus volume data is plotted below (Figure 3-33)

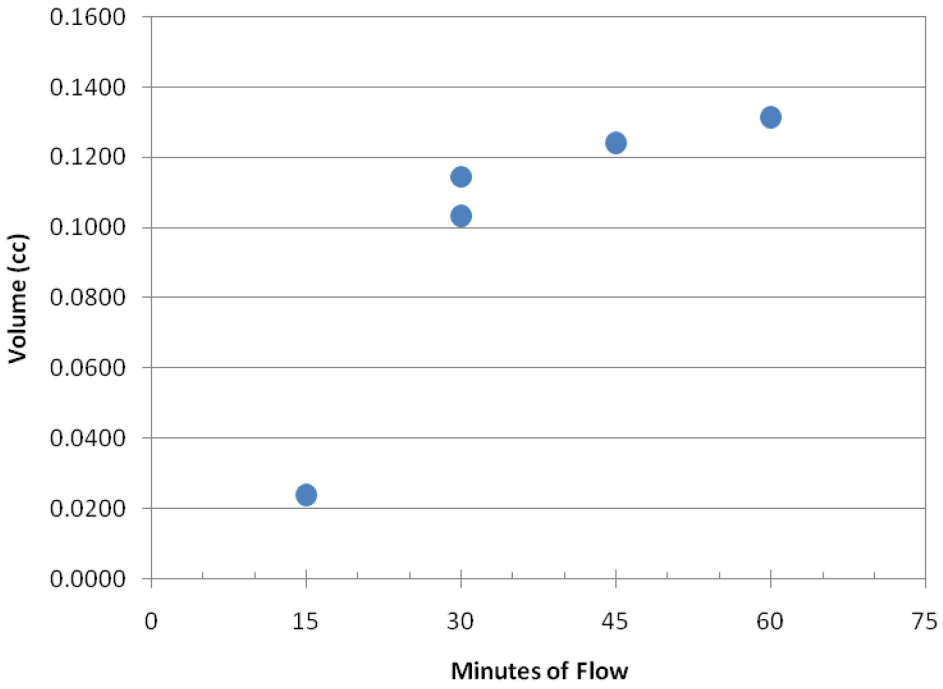

Figure 3-33: This graph illustrates the volume of the formed thrombus from each flow time.

Figure 3-33 indicates that the thrombus downstream of the backward facing step in the model grows quickly at first. Between 15 minutes and 30 minutes, the thrombus experiences rapid growth to just more than 0.1 cc. Thrombus growth then slows after 30 minutes. This indicates that any further thrombus growth may be inhibited by the fluid flow jet as the thrombus has filled the majority of the downstream recirculation area for this particular flow rate. Once the recirculation area downstream of the backward facing step is occupied by the thrombus, the fluid flow would wash away any further thrombus growth. The size of the area of recirculation is highly dependent on the Reynolds number of the model and consequentially the fluid flow's point of reattachment. This study's results only includes one low time flow data set at 15 minutes at a Reynolds number of 1000. These results thus cannot be firmly asserted without further future data collection between 0 and 30 minutes of flow time and at various Reynolds numbers.

Chapter 4

4.1 Conclusions

This study provides a better understanding of the conditions under which thrombi form. Using an *in vitro* backward facing step model and flow loop, various thrombi were generated at a physiologically relevant flow rate (0.79 L/min). Thrombi formation was observed by imaging the developing thrombus at 15, 30, 45, and 60 minutes. These thrombi were observed with three-dimensional MRI and reconstructed for later CFD simulations.

The size and volume of the thrombi are correlated with the amount of time the blood flows through the model. Thrombus growth is variable during the time period studies with rapid growth apparent between 15 and 30 minutes of blood flow. After 30 minutes, thrombus growth is slowed as the fluid recirculation zone is mostly filled by the thrombus. Repetition of these studies should be performed to further confirm these conclusions.

4.2 Future Work

The meshes generated from this project will be used in CFD simulations. These simulations will be used to determine the fluid flow characteristics and shear stresses acting on the formed thrombi. CFD will also try and model the growth of the forming thrombi over time. This will be possible by analyzing the changes in the MRI derived meshes this project created at 15, 30, 45, and 60 minutes.

Experimentally, we will continue to investigate the formation of thrombi downstream of the backward facing step. This will involve varying the flow rate to simulate blood flow at a heart rate of 50 bpm (0.39 L/min) and 100 bpm (1.5 L/min).

An additional backward facing step model (Figure 4-1) was designed in this

project for future research use. This model was a revision of the first and incorporated several improvements. The primary change involved moving the screw assembly points of the two model pieces upstream of the step location and a reduction in the overall model size.

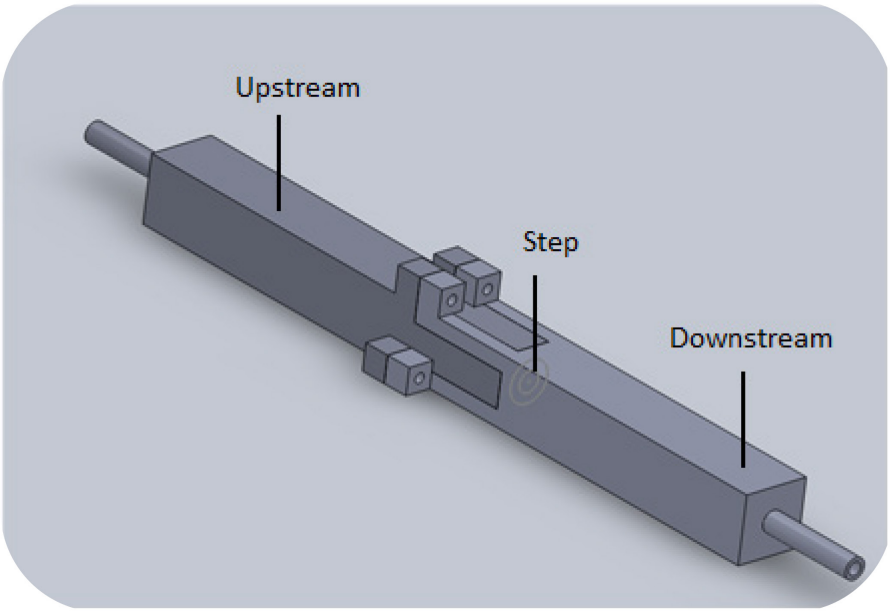

Figure 4-1: Revised, smaller model

This reduction in size also focused the model on smaller thrombi and reduced the volume of the flow loop by a small amount. Moving these attachment points created a more homogenous model around the primary area of interest, just downstream of the backward facing step. By having a more uniform segment of acrylic in this area rather than protrusions of acrylic for the screw attachments, an increase in the MRI signal-to-noise ratio was possible. This increase in signal-to-noise ratio allows for better imaging in this area [34]. A second major change involved reducing the size of the inner diameter of the model channel from 10 mm to 6 mm. This reduction in size allowed for the use of a smaller radio frequency coil around the model, again increasing the MRI imaging quality of the formed thrombus. The attachment of upstream and downstream tubing was simplified by the size reduction since the 6.35 mm tubing could connect directly to the

model without an adapter.

This project considered a small number of variables that affect thrombosis. There are many different questions that can be further investigated with this research to better understand thrombi formation.

Bibliography

[1] Daneshmand, M. A., Rajagopal, K., Lima, B., Khorram, N., Blue, L. J., Lodge, A. J., Hernandez, A. F., Rogers, J. G., and Milano, C. A., 2010, "Left Ventricular Assist Device Destination Therapy Versus Extended Criteria Cardiac Transplant," The Annals of Thoracic Surgery, 89(4), pp. 1205-1210.

[2] Fraser, K., Taskin, M. E., Griffith, B., and Wu, Z., 2011, "The use of computational fluid dynamics in the development of ventricular assist devices," Medical engineering & physics, 33(3), pp. 263-280.

[3] Lloyd-Jones, D., Adams, R. J., Brown, T. M., Carnethon, M., Dai, S., De Simone, G., Ferguson, T. B., Ford, E., Furie, K., Gillespie, C., Go, A., Greenlund, K., Haase, N., Hailpern, S., Ho, P. M., Howard, V., Kissela, B., Kittner, S., Lackland, D., Lisabeth, L., Marelli, A., mcdermott, M. M., Meigs, J., Mozaffarian, D., Mussolino, M., Nichol, G., Roger, V. L., Rosamond, W., Sacco, R., Sorlie, P., Thom, T., Wasserthiel-Smoller, S., Wong, N. D., and Wylie-Rosett, J., 2010, "Heart disease and stroke statistics--2010 update: a report from the American Heart Association," Circulation, 121(7), pp. E46-e215.

[4] Roger, V. L., Go, A. S., Lloyd-Jones, D. M., Adams, R. J., Berry, J. D., Brown, T. M., Carnethon, M. R., Dai, S., de Simone, G., Ford, E. S., Fox, C. S., Fullerton, H. J., Gillespie, C., Greenlund, K. J., Hailpern, S. M., Heit, J. A., Ho, P. M., Howard, V. J., Kissela, B. M., Kittner, S. J., Lackland, D. T., Lichtman, J. H., Lisabeth, L. D., Makuc, D. M., Marcus, G. M., Marelli, A., Matchar, D. B., mcdermott, M. M., Meigs, J. B., Moy, C. S., Mozaffarian, D., Mussolino, M. E., Nichol, G., Paynter, N. P., Rosamond, W. D., Sorlie, P. D., Stafford, R. S., Turan, T. N., Turner, M. B., Wong, N. D., and Wylie-Rosett, J., 2010, "Heart Disease and Stroke Statistics--2011 Update: A Report From the American Heart Association," Circulation, 123(4), pp. E18-e209.

[5] Gemmato, C., Forrester, M., Myers, T., Frazier, O., and Cooley, D., 2005, "Thirty-five years of mechanical circulatory support at the Texas Heart Institute - An updated overview," Texas Heart Institute journal, 32(2), pp. 168-177.

[6] Moazami, N., Roberts, K., Argenziano, M., Catanese, K., Mohr, J. P., Rose, E. A., and Oz, M. C., 1997, "Asymptomatic microembolism in patients with long-term ventricular assist support," Asaio Journal, 43(3), pp. 177-180.

[7] Schmid, C., Weyand, M., Nabavi, D. G., Hammel, D., Deng, M. C., Ringelstein, E. B., and Scheld, H. H., 1998, "Cerebral and systemic embolization during left ventricular support with the Novacor N100 device," Annals of Thoracic Surgery, 65(6), pp. 1703-1710.

[8] Notzold, A., Droste, D. W., Hagedorn, G., Berndt, S., Kaps, M., Graf, B., and Sievers, H. H., 1997, "Circulating microemboli in patients after aortic valve replacement with pulmonary autografts and mechanical valve prostheses," Circulation, 96(6), pp. 1843-1846.

[9] Garg, S., and Serruys, P. W., 2010, "Coronary stentslooking Forward," Journal of the American College of Cardiology, 56(10), pp. S43-S78.

[10] Edmunds, L. H., 1996, "Is prosthetic valve thrombogenicity related to design or material?," Texas Heart Institute journal, 23(1), pp. 24-27.

[11] Gorbet, M., 2004, "Biomaterial-associated thrombosis: roles of coagulation factors, complement, platelets and leukocytes," Biomaterials, 25(26), pp. 5681-

5703.
[12] Maegdefessel, L., Linde, T., Krapiec, F., Hamilton, K., Steinseifer, U., van Ryn, J., Raaz, U., Buerke, M., Werdan, K., and Schlitt, A., 2010, "In vitro comparison of dabigatran, unfractionated heparin, and low-molecular-weight heparin in preventing thrombus formation on mechanical heart valves☆," Thrombosis Research, 126(3), pp. E196-e200.
[13] Gentry, P., 2004, "Comparative aspects of blood coagulation," The Veterinary Journal, 168(3), pp. 238-251.
[14] Fraser, K. H., Taskin, M. E., Griffith, B. P., and Wu, Z. J., 2011, "The use of computational fluid dynamics in the development of ventricular assist devices," Medical Engineering & Physics, 33(3), pp. 263-280.
[15] Bennett, P., Silverman, S., Gill, P., and Lip, G., 2009, "Peripheral arterial disease and Virchow's triad," Thrombosis and haemostasis, 101(6), pp. 1032-1040.
[16] Spittell, J., 1963, "Thrombophlebitis And Pulmonary Embolism," Circulation, 27(5), p. 976.
[17] Windberger, U., Bartholovitsch, A., Plasenzotti, R., Korak, K. J., and Heinze, G., 2003, "Whole blood viscosity, plasma viscosity and erythrocyte aggregation in nine mammalian species: reference values and comparison of data," Experimental Physiology, 88(3), pp. 431-440.
[18] Szczeklik, A., Krzanowski, M., Gora, P., and Radwan, J., 1992, "Antiplatelet Drugs And Generation Of Thrombin In Clotting Blood," Blood, 80(8), pp. 2006-2011.
[19] Reynolds, L. O., Newren, W. H., Scolio, J. F., and Miller, I. F., 1993, "A Model For Thromboembolization On Biomaterials," Journal of Biomaterials Science-Polymer Edition, 4(5), pp. 451-465.
[20] Wilson, R. S., Marmur, A., and Cooper, S. L., 1986, "A Model Of Deposition And Embolization Of Proteins And Platelets On Biomaterial Surfaces," Annals of Biomedical Engineering, 14(4), pp. 383-400.
[21] Slack, S. M., Bohnert, J. L., And Horbett, T. A., 1987, "The Effects Of Surface-Chemistry And Coagulation-Factors On Fibrinogen Adsorption From Plasma," Annals Of The New York Academy Of Sciences, 516, Pp. 223-243.
[22] Tepe, G., Wendel, H., Khorchidi, S., Schmehl, J., Wiskirchen, J., Pusich, B., Claussen, C., and Duda, S., 2002, "Thrombogenicity of Various Endovascular Stent Types: An In Vitro Evaluation," Journal of Vascular and Interventional Radiology, 13(10), pp. 1029-1035.
[23] Cengel, Y. A., and Cimbalam, J. M., 2008, Fluid Mechanics Fundamentals and Applications, mcgraw Hill, New York, NY.
[24] Armaly, B., Durst, F., Pereira, J., and Schonung, B., 1983, "Experimental And Theoretical Investigation Of Backward-Facing Step Flow," Journal of Fluid Mechanics, 127(Feb), pp. 473-496.
[25] Barkley, D., Gomes, M. G. M., and Henderson, R. D., 2002, "Three-dimensional instability in flow over a backward-facing step," Journal of Fluid Mechanics, 473.
[26] Beaudoin, and J., 2004, "Three-dimensional stationary flow over a backward-facing step," European Journal of Mechanics - B/Fluids, 23(1), pp. 147-155.
[27] Rani, H. P., Sheu, T. W. H., and Tsai, E. S. F., 2007, "Eddy structures in a transitional backward-facing step flow," Journal of Fluid Mechanics, 588.
[28] Biswas, G., Breuer, M., and Durst, F., 2004, "Backward-Facing Step Flows for Various Expansion Ratios at Low and Moderate Reynolds Numbers," Journal of

Fluids Engineering, 126(3), p. 362.
[29] Gresho, P., Gartling, D., Torczynski, J., Cliffe, K., Winters, K., and Garratt, T., 1993, "Is The Steady Viscous Incompressible 2-Dimensional Flow Over A Backward-Facing Step At Re=800 Stable," International journal for numerical methods in fluids, 17(6), pp. 501-541.
[30] Chandler, A. B., 1958, "Invitro Thrombotic Coagulation Of The Blood - A Method For Producing A Thrombus," Laboratory Investigation, 7(2), pp. 110-114.
[31] Stringer, H., Vanswieten, P., Heijnen, H., Sixma, J., and Pannekoek, H., 1994, "Plasminogen-Activator Inhibitor-1 Released From Activated Platelets Plays A Key Role In Thrombolysis Resistance - Studies With Thrombi Generated In The Chandler Loop," Arteriosclerosis and thrombosis, 14(9), pp. 1452-1458.
[32] Fayad, Z. A., Fallon, J. T., Shinnar, M., Wehrli, S., Dansky, H. M., Poon, M., Badimon, J. J., Charlton, S. A., Fisher, E. A., Breslow, J. L., and Fuster, V., 1998, "Noninvasive in vivo high-resolution magnetic resonance imaging of atherosclerotic lesions in genetically engineered mice," Circulation, 98(15), pp. 1541-1547.
[33] Johnstone, M. T., Botnar, R. M., Perez, A. S., Stewart, R., Quist, W. C., Hamilton, J. A., and Manning, W. J., 2001, "In Vivo Magnetic Resonance Imaging of Experimental Thrombosis in a Rabbit Model," Arteriosclerosis, Thrombosis, and Vascular Biology, 21(9), pp. 1556-1560.
[34] Taylor, C. A., and Draney, M. T., 2004, "Experimental and Computational Methods in Cardiovascular Fluid Mechanics," Annual Review of Fluid Mechanics, 36(1), pp. 197-231.
[35] Sobey, I. J., 1982, "Oscillatory Flows At Intermediate Strouhal Number In Asymmetric Channels," Journal of Fluid Mechanics, 125(Dec), pp. 359-373.

Appendix

MatLab Code for MRI Data Conversion--Adapted from Dr. Thomas Neuberger

```
%ge3d_tn
%reads and transforms data from a 3d gradient echo sequence
clear all;
close all;
tic
%% zero filling factor
zf=2
%% circular shifts of the image and intensity scaling
list=[  1,   2,   3]
xxx=[   0,   0,   0]
yyy=[ -60, -60, -60]
zzz=[  80,  80,  80]
aaa=[0.002,0.002,0.002]
pathname1=(['/gpfs/home/atc5049/work/MatLab_and_Data/s_20110210_01_30min_time
/data/ge3d_02.fid/'])
pathname=pathname1
%bigger xx shifts to the right
%larger yy shifts to the bottom
d=1:1
%for d=1:1%size(list,2)
xx=xxx(d)
yy=yyy(d)
zz=zzz(d)
aa=aaa(d)
filename = ('fid');
dateiname=([pathname 'procpar'])
%% create info file
info=read_info_28102010([pathname 'procpar'],zf,aa,xx,yy,zz);
cd(pathname);
pwd
%% read raw data (fid file)
fid=fopen(strcat(pathname,filename),'r','b');
% offset for file header
offset1=32;
% offset for data block header
offset2=28;
fseek(fid,offset1+offset2,0);
raw=fread(fid,inf,'float32');
fclose(fid);
rawsize=size(raw)
'reading raw data done'
%% rename  #read, #phase and #phase3d
readpoints=info.ReadPoints/2
phasepoints=info.PhasePoints
```

```
phasepoints3d =info.PhasePoints3D
petable=info.petable
seqcon=info.seqcon
%% create recomatrix
slice2=zeros(readpoints,phasepoints,phasepoints3d);
%% combine data into complex data sets and do the sorting
   currIndex=0;
   for k=1:phasepoints3d
         for i=1:phasepoints
%          for l=1:phasepoints3d*phasepoints
            for l=1:readpoints
             currIndex = currIndex + 1;
                                  dataR(l) = raw(currIndex);
             currIndex = currIndex + 1;
                                  dataI(l) = raw(currIndex);
%              slice2(l,k) = (dataR(l) + dataI(l) * j);
             slice2(l,i,k) = (dataR(l) + dataI(l) * j);
            end
         end
%for seqcon=nccsn
currIndex =currIndex + offset2/4.;
   end
currIndex
'sorting done'
%slice2=reshape(slice1,[readpoints phasepoints phasepoints3d]);
%slice2=slice1;
clear slice1
clear raw
%% figure out petable
pe_siz=size(petable)
if pe_siz(2) > 0
   len=size(petable);
   frac=petable((len(2)-2):len(2));
   frac=str2num(frac);
   phasepoints=phasepoints/frac*1000
end
%% fourier transformation
'start fft'
Image2=abs(fftshift(ifftn(slice2,[zf*readpoints, zf*phasepoints, zf*phasepoints3d])));
'fft done'
%% circular shift
Image=circshift(Image2,[xx yy zz]);
figure(1); imshow(squeeze(Image(readpoints/2,:,:)),[0,aa])

%% writing bitmaps
%%%%%%%%%%%%%%%%%%%% read direction %%%%%%%%%%%%
%cd 'H:/3Dimages/';
%mkdir(study);
```

```
%cd (study);
%cd(char(pathname(loop)));
cd(pathname);
mkdir(['Images_read_zf_' num2str(zf)]);
cd (['Images_read_zf_' num2str(zf)])
%mkdir('Images_read');
%cd 'Images_read'
'writing read - images'
for n=1:readpoints*zf %phasepoints %readpoints
%aa=.13
ds=2;
n;
if  n < 10
mwrite(abs(squeeze(Image(n,:,:)))/aa,strcat('image_',num2str(aa),'_000',num2str(n),'.bmp'
),'bmp')
%if  (2*n + ds) < 10
%
imwrite(abs(squeeze(Image(n+1,:,:)))/aa,strcat('image_',num2str(aa),'_000',num2str(2*n
+ ds),'.bmp'),'bmp')
end
if  n < 100 && n > 9
imwrite(abs(squeeze(Image(n,:,:)))/aa,strcat('image_',num2str(aa),'_00',num2str(n),'.bmp'
),'bmp')
%if  (2*n + ds +6) < 99 && (2*n + ds) > 9
%    imwrite(abs(squeeze(Image(n,:,:)))/aa,strcat('image_',num2str(aa),'_00',num2str(2*n
+ ds),'.bmp'),'bmp')
end
if  n  < 1000 && n > 99
imwrite(abs(squeeze(Image(n,:,:)))/aa,strcat('image_',num2str(aa),'_0',num2str(n),'.bmp'),'
bmp')
%if  (2*n + ds) < 999 && (2*n + ds) > 99
%    imwrite(abs(squeeze(Image(n,:,:)))/aa,strcat('image_',num2str(aa),'_0',num2str(2*n +
ds),'.bmp'),'bmp')
end
if  n  < 10000 && n > 999
imwrite(abs(squeeze(Image(n,:,:)))/aa,strcat('image_',num2str(aa),'_',num2str(n),'.bmp'),'b
mp')
%if  (2*n + ds) < 999 && (2*n + ds) > 99
%    imwrite(abs(squeeze(Image(n,:,:)))/aa,strcat('image_',num2str(aa),'_0',num2str(2*n +
ds),'.bmp'),'bmp')
end
end
%imwrite(abs(Image)/10,strcat('image_000',num2str(n+1),'.bmp'),'bmp')
cd '..'
maximum=max(max(max(Image)))
%%%%%%%phase direction %%%%%%%%%%%%%%%%%
% % % mkdir(['Images_phase_zf_' num2str(zf)]);
% % % cd (['Images_phase_zf_' num2str(zf)])
```

```
% % % %mkdir('Images_phase');
% % % %cd 'Images_phase'
% % % 'writing phase - images'
% % % for n=1:phasepoints*zf  %phasepoints %readpoints
% % % %aa=.13
% % % ds=2;
% % % n;
% % % if  n < 10
% % %
imwrite(abs(squeeze(Image(:,n,:)))/aa,strcat('image_',num2str(aa),'_000',num2str(n),'.bm
p'),'bmp')
% % % %if  (2*n + ds) < 10
% % % %
imwrite(abs(squeeze(Image(n+1,:,:)))/aa,strcat('image_',num2str(aa),'_000',num2str(2*n
+ ds),'.bmp'),'bmp')
% % % end
% % % if  n < 100 && n > 9
% % %
imwrite(abs(squeeze(Image(:,n,:)))/aa,strcat('image_',num2str(aa),'_00',num2str(n),'.bmp'
),'bmp')
% % % %if  (2*n + ds +6) < 99 && (2*n + ds) > 9
% % % %
imwrite(abs(squeeze(Image(n,:,:)))/aa,strcat('image_',num2str(aa),'_00',num2str(2*n +
ds),'.bmp'),'bmp')
% % % end
% % % if  n  < 1000 && n > 99
% % %
imwrite(abs(squeeze(Image(:,n,:)))/aa,strcat('image_',num2str(aa),'_0',num2str(n),'.bmp'),'
bmp')
% % % %if  (2*n + ds) < 999 && (2*n + ds) > 99
% % % %
imwrite(abs(squeeze(Image(n,:,:)))/aa,strcat('image_',num2str(aa),'_0',num2str(2*n +
ds),'.bmp'),'bmp')
% % % end
% % % if  n  < 10000 && n > 999
% % %
imwrite(abs(squeeze(Image(:,n,:)))/aa,strcat('image_',num2str(aa),'_',num2str(n),'.bmp'),'b
mp')
% % % %if  (2*n + ds) < 999 && (2*n + ds) > 99
% % % %
imwrite(abs(squeeze(Image(n,:,:)))/aa,strcat('image_',num2str(aa),'_',num2str(2*n +
ds),'.bmp'),'bmp')
% % % end
% % %
% % % end
% % % %imwrite(abs(Image)/10,strcat('image_000',num2str(n+1),'.bmp'),'bmp')
% % % cd '..'
% % %
```

```
% % %
%%%%%%%%%%%%%%%%%%%%%%%%%%%%%%%%%%%%%%%%%%%%%%%
phase2 direction %%%%%%%%%%%%%%%%%%
% % % mkdir(['Images_phase3d_zf_' num2str(zf)]);
% % % cd (['Images_phase3d_zf_' num2str(zf)])
% % % %mkdir('Images_phase3d');
% % % %cd 'Images_phase3d'
% % %
% % % %mkdir('Images_phase3d');
% % % %cd 'Images_phase3d'
% % % %'read um 80 gekuerzt!!!!!!!!'
% % % 'writing phase3d - images'
% % % for n=1:phasepoints3d*zf %phasepoints %readpoints
% % % %aa=.13
% % % ds=2;
% % % n;
% % % if  n < 10
% % %
imwrite(abs(squeeze(Image(:,:,n)))/aa,strcat('image_',num2str(aa),'_000',num2str(n),'.bm
p'),'bmp')
% % % %if  (2*n + ds) < 10
% % % %
imwrite(abs(squeeze(Image(n+1,:,:)))/aa,strcat('image_',num2str(aa),'_000',num2str(2*n
+ ds),'.bmp'),'bmp')
% % % end
% % % if  n < 100 && n > 9
% % %
imwrite(abs(squeeze(Image(:,:,n)))/aa,strcat('image_',num2str(aa),'_00',num2str(n),'.bmp'
),'bmp')
% % % %if  (2*n + ds +6) < 99 && (2*n + ds) > 9
% % % %
imwrite(abs(squeeze(Image(n,:,:)))/aa,strcat('image_',num2str(aa),'_00',num2str(2*n +
ds),'.bmp'),'bmp')
% % % end
% % % if  n  < 1000 && n > 99
% % %
imwrite(abs(squeeze(Image(:,:,n)))/aa,strcat('image_',num2str(aa),'_0',num2str(n),'.bmp'),'
bmp')
% % % %if  (2*n + ds) < 999 && (2*n + ds) > 99
% % % %
imwrite(abs(squeeze(Image(n,:,:)))/aa,strcat('image_',num2str(aa),'_0',num2str(2*n +
ds),'.bmp'),'bmp')
% % % end
% % % if  n  < 10000 && n > 999
% % %
imwrite(abs(squeeze(Image(:,:,n)))/aa,strcat('image_',num2str(aa),'_',num2str(n),'.bmp'),'b
mp')
% % % %if  (2*n + ds) < 999 && (2*n + ds) > 99
```

```
% % % %
imwrite(abs(squeeze(Image(n,:,:)))/aa,strcat('image_',num2str(aa),'_',num2str(2*n +
ds),'.bmp'),'bmp')
% % % end
% % %
% % % end
% % % %imwrite(abs(Image)/10,strcat('image_000',num2str(n+1),'.bmp'),'bmp')
% % % cd '..'
% % %
%clear 'Image'
%end
%save -v7.3 ('Image.mat', 'Image')
%save  ('Image.mat', 'Image')
%end
%end
toc
```

ANDREW T. CATHERINE

15 South Eighth Street Philipsburg, PA 16866
atcatherine@psu.com
(814) 422-5049

Objective: To use my background and research experience in Bioengineering to pursue a career in medicine.

Education:

The Pennsylvania State University

- Major: Bioengineering
- Minor: Information Science Technology in Health Policy Administration
- Schreyer Honors Scholar
- Graduation: May 2011

Research Experience:

Research Assistant to Dr. Keefe Manning (Penn State, Assistant Professor of Bioengineering) 2009-Present

- Studied the Computational Fluid Dynamics of a Backwards Facing Step and Thrombus Formation
- Analyzed the fluid mechanics involved in the backward facings step geometry

Research Assistant to Dr. Amy Parente (Penn State Altoona, Assistant Professor of Biochemistry) 2007-2009

- Participated in development and testing of DNA sequences using spectrophotometric techniques in collaboration with Dr. Philip Bevilacqua's lab (Penn State University Park)
- Developed and maintained Dr. Parente's web page
- Presented a project poster at the Pennsylvania Academy of Sciences Conference April 2009

Research Participant at SEA Education Association under the advisement of Dr. Giora Prokuwoski (Woods Hole Oceanographic Institution) May- July 2009

- Studied the Effects of Dissolved Inorganic Carbon on the Abundance of Foraminifera and Pteropods
- Participated in summer research cruise from Honolulu, HI to San Francisco, CA
- Collected and chemically analyzed water samples from a depth of 3000 meters to the water surface

Activities and Interests:

- Active member of Tau Beta Pi Engineering Honor Society 2009- present
- Lion Ambassador at Penn State Altoona 2007-2009
- Member of Penn State Altoona's Honor Leadership Team 2007-2009

Awards:

- Eagle Scout
- Member of : Phi Kappa Phi, Omicron Delta Kappa, and Alpha Lambda Delta

Work Experience:

- Pharmacy Technician at Grattan’s Pharmacy 2005-2007
- Emergency Medical Technician at University Health Services Penn State University 2007- Present